processes

MDPI

Article

Thermodynamically Efficient, Low-Emission Gas-to-Wire for Carbon Dioxide-Rich Natural Gas: Exhaust Gas Recycle and Rankine Cycle Intensifications

Israel Bernardo S. Poblete, José Luiz de Medeiros * and Ofélia de Queiroz F. Araújo

Chemistry School, Centro de Tecnologia, E, Federal University of Rio de Janeiro, Ilha do Fundão, Rio de Janeiro 21941-909, RJ, Brazil; ibspoblete@eq.ufrj.br (I.B.S.P.); ofelia@eq.ufrj.br (O.d.Q.F.A.)
* Correspondence: jlm@eq.ufrj.br

Abstract: Onshore gas-to-wire is considered for 6.5 $MMSm^3/d$ of natural gas, with 44% mol carbon dioxide coming from offshore deep-water oil and gas fields. Base-case GTW-CONV is a conventional natural gas combined cycle, with a single-pressure Rankine cycle and 100% carbon dioxide emissions. The second variant, GTW-CCS, results from GTW-CONV with the addition of post-combustion aqueous monoethanolamine carbon capture, coupled to carbon dioxide dispatch to enhance oil recovery. Despite investment and power penalties, GTW-CCS generates both environmental and economic benefits due to carbon dioxide's monetization for enhanced oil production. The third variant, GTW-CCS-EGR, adds two intensification layers over GTW-CCS, as follows: exhaust gas recycle and a triple-pressure Rankine cycle. Exhaust gas recycle is a beneficial intensification for carbon capture, bringing a 60% flue gas reduction (reduces column's diameters) and a more than 100% increase in flue gas carbon dioxide content (increases driving force, reducing column's height). GTW-CONV, GTW-CCS, and GTW-CCS-EGR were analyzed on techno-economic and environment–thermodynamic grounds. GTW-CCS-EGR's thermodynamic analysis unveils 807 MW lost work (79.8%) in the combined cycle, followed by the post-combustion capture unit with 113 MW lost work (11.2%). GTW-CCS-EGR achieved a 35.34% thermodynamic efficiency, while GTW-CONV attained a 50.5% thermodynamic efficiency and 56% greater electricity exportation. Although carbon capture and storage imposes a 35.9% energy penalty, GTW-CCS-EGR reached a superior net value of 1816 MMUSD thanks to intensification and carbon dioxide monetization, avoiding 505.8 t/h of carbon emissions (emission factor 0.084 t^{CO2}/MWh), while GTW-CONV entails 0.642 t^{CO2}/MWh.

Keywords: natural gas; gas-to-wire; post-combustion carbon capture; exhaust gas recycle; CCS; thermodynamic analysis; multi-criteria analysis; process intensification; carbon dioxide monetization

check for updates

Citation: Poblete, I.B.S.; de Medeiros, J.L.; Araújo, O.d.Q.F. Thermodynamically Efficient, Low-Emission Gas-to-Wire for Carbon Dioxide-Rich Natural Gas: Exhaust Gas Recycle and Rankine Cycle Intensifications. *Processes* **2024**, *12*, 639. https://doi.org/10.3390/pr12040639

Academic Editors: Inês Portugal, Carlos Manuel Silva and José Aniceto

Received: 25 February 2024
Revised: 19 March 2024
Accepted: 20 March 2024
Published: 22 March 2024

Copyright: © 2024 by the authors. Licensee MDPI, Basel, Switzerland. This article is an open access article distributed under the terms and conditions of the Creative Commons Attribution (CC BY) license (https://creativecommons.org/licenses/by/4.0/).

1. Introduction

Greenhouse gas concerns and the increasing global energy demand have driven the deployment of renewable energy sources, but this transition is not immediate and bridge fuels are necessary. This is the case of natural gas (NG), whose high hydrogen/carbon ratio has entailed NG recognition as a bridge fuel for the transition to a low-carbon economy. Recently, large NG reserves with high carbon dioxide (CO_2) content have been found in remote offshore fields, such as the offshore Brazilian pre-salt oil and gas fields that have CO_2-rich NG at a high gas/oil ratio, challenging NG-processing technologies. Thus, low-emission technologies are necessary to adopt CO_2-rich NG in energy grids under carbon constraints [1].

To face the rise of the atmospheric CO_2 content and to reconcile the growing global energy demand with a low-carbon economy, climate agreements have appeared in the last two decades—the Kyoto Protocol [2], European Union Emissions Trading Scheme [3], and Paris Agreement [4]—recognizing the inappropriateness of current energy sources and the necessary, immediate transition to a low-carbon economy.

To implement low-emission, CO_2-rich NG power plants, CO_2 must be removed from flue gas using carbon capture and storage (CCS) [5]. This captured CO_2 can be monetized if injected in oil fields for enhanced oil recovery (EOR), while being geologically stored [6].

1.1. Low-Emission, CO_2-Rich Natural Gas Combined Cycle Power Plants

Considering gas-to-wire schemes for CO_2-rich NG, the best thermodynamic yield is achieved by NG combined cycle (NGCC) plants. NGCC combines a Brayton cycle (gas turbines) with a Rankine Cycle (steam turbines) to achieve a high overall thermodynamic yield [7]. A low-emission NGCC, firing CO_2-rich NG, demands the implementation of CCS alternatives [8], such as post-combustion membrane permeation [9], post-combustion chemical absorption [10], post-combustion ionic liquid absorption [11], post-combustion carbonation–calcination capture [12], pre-combustion capture [13], and oxy-combustion technologies [14]. Several comparisons of CCS schemes are found elsewhere [15].

The most mature CCS technology is post-combustion capture via chemical absorption with aqueous monoethanolamine or PCC-MEA [16]. The major drawbacks of PCC-MEA are the high heat ratio—3 MJ/kg^{CO2} to 4 MJ/kg^{CO2}—for stripping CO_2 [17], as well as its liberation at low pressures [18]. Peeters et al. [19] performed a techno-economic analysis of NGCC with PCC-MEA showing how solvent loadings affect the heat ratio. Tait et al. [20] techno-economically analyzed a pilot-scale NGCC with PCC-MEA. Schach et al. [21] evaluated PCC-MEA alternatives, showing that two strippers and an intercooled absorber can save the power penalty by 4% to 7%. Luo and Wang [22] modeled NGCC with PCC-MEA. Bao et al. [23] proposed an NGCC fed with liquefied NG, reaching a 2.51% higher thermodynamic yield and a 7.9% lower power penalty.

Cormos [24] investigated an NGCC with post-combustion capture via calcium looping that reached EUR 56.91/MWh electricity cost. Garcia et al. [25] proposed an NGCC with post-combustion capture via lithium-based sorbents (Li_4SiO_4/Li_2CO_3), achieving a similar thermodynamic yield to that of NGCC coupled to PCC-MEA. Zhang et al. [26] presented an NGCC with novel CCS via solid amine adsorbents for flue gas with 15% v/v CO_2. Roussanaly et al. [27] techno-economically analyzed onshore/offshore NGCC-CCS, achieving *95* and USD 258/MWh electricity costs, respectively.

Gas-to-wire with CCS has been consolidated as being viable and low emission in both offshore and onshore scenarios [28]. Flórez-Orrego et al. [29] studied gas-to-wire in offshore power hubs for supplying electricity to various floating rigs. Orisaremi et al. [30] applied gas-to-wire to reduce gas flaring in oil-producing sites. Jokar et al. [31] proposed gas-to-wire as a reliable and profitable option for flaring prevention.

1.2. Exhaust Gas Recycle

Exhaust gas recycle (EGR) is primarily used for nitrogen oxide reduction in diesel engines [32]. EGR returns a fraction of cooled flue gas to the air intake system, reducing the air-to-fuel excess ratio, consequently reducing O_2 availability in the combustion and lowering NO_x formation. EGR injects more CO_2 and H_2O—which have a higher molar heat capacity than air—in the air–fuel mixture, reducing air excess for temperature control and increasing flue gas CO_2 content [33]. This last aspect suggests using EGR as an NGCC-CCS intensification [34,35]. Ali et al. [36] showed that recycling 50% of flue gas in an NGCC-CCS entails lower energy penalties. Lee et al. [37] indicated that excessive EGR can hinder stable gas turbine operations, reducing the net power due to a non-optimal oxygen/fuel ratio.

1.3. Thermodynamic Analysis of Processes

Exergy is the maximum available work that can be extracted from a material stream, as it is freed, to reach equilibrium with a ground-level reference environmental reservoir [38]. Although thermodynamic and exergy efficiencies are directly related, and despite the equivalence between thermodynamic analysis and exergy analysis, they are not the same object. Thermodynamic analysis is absolute and is fully described in the context of the second law of thermodynamics, whereas exergy analysis works with a datum reference

environmental reservoir [39]. Exergy analysis has been widely explored in the literature to investigate the sustainability of processes in terms of exergy efficiencies that measure the extent of resource degradation in the process. Meanwhile, thermodynamic analysis is less commonly used, but is independent of datum reservoirs and can generate similar results.

Geuzebroek et al. [40] performed an exergy analysis of an NGCC with PCC-MEA, showing that the CO_2 absorber and stripper are significant exergy sinks. Gulen et al. [41] performed an exergy analysis of the Rankine cycle of an NGCC, evincing a 71% exergy efficiency. Brigagão et al. [42] performed an exergy analysis of air pre-purification with supersonic separators, finding a 60% exergy efficiency. Cruz et al. [43] presented an exergy comparison between arrangements of multiple-paralleled and single-shaft compressors on offshore rigs exploring CO_2-rich NG. The exergy efficiencies at 25% and 100% gas loads were 49% and 83% for single-shaft and 80% and 88% for multiple-paralleled. Wiesberg et al. [44] performed an exergy analysis of CCS and carbon capture and utilization (CCU) for methanol production via CO_2 hydrogenation and via synthesis gas from bi-reforming. The exergy efficiencies were 66.3% and 55.8%, respectively, for CCU and 44.8% for CCS. In a study with a large-scale sugarcane biorefinery, Milão et al. [45] reported an 11.1% thermodynamic efficiency for the ethanol separation system with a Petlyuk column and 7.65% for heat-integrated distillation. Talebizadehsardari et al. [46] reported exergy efficiencies of 73.7% for an organic Rankine cycle heated with exhaust gas and 51.9% for an organic Rankine cycle integrated with CCS. Amrollahi et al. [47] performed an exergy analysis of an NGCC with PCC-MEA, finding a 31.6% exergy efficiency. Minutillo et al. [48] conducted an exergy analysis of hydrogen production from biogas, achieving a 59.4% exergy efficiency.

1.4. The Present Work

This work approaches onshore gas-to-wire as a low-emission monetization strategy for CO_2-rich NG from offshore, remotely located oil/gas fields. The low-emission GTW-CCS alternative integrating gas-to-wire with PCC-MEA was assessed first. Then, GTW-CCS was intensified through EGR implementation with a triple-pressure Rankine cycle, creating the intensified low-emission GTW-CCS-EGR. GTW-CCS and GTW-CCS-EGR were techno-economically, environmentally, and thermodynamically evaluated and compared to the conventional gas-to-wire GTW-CONV. CCS directly impacts power generation and, consequently, also impacts economic performance and thermodynamic efficiency, while EGR alleviates the CCS penalty. The evaluation of these conjugated effects coupled to the environmental analysis and second law analysis of full large-scale intensified GTW-CCS-EGR fed with CO_2-rich NG is the spirit of this work, a proposal inexistent in the literature.

2. Methods

Three onshore gas-to-wire systems—GTW-CONV, GTW-CCS, and GTW-CCS-EGR—firing CO_2-rich NG were designed in Aspen-HYSYS and assessed on techno-economic and environment–thermodynamic grounds. GTW-CONV is a conventional NGCC without CCS. GTW-CCS is an NGCC coupled to PCC-MEA, and performs both CO_2 compression and dehydration. GTW-CCS-EGR is GTW-CCS intensified with EGR and a triple-pressure Rankine cycle.

2.1. GTW-CONV, GTW-CCS, and GTW-CCS-EGR

Figure 1 presents the gas-to-wire concepts contemplated here. GTW-CONV fires CO_2-rich NG comprising (i) an NGCC with gas turbines GE9F.05 integrated to a heat recovery steam generator (HRSG) and a single-pressure Rankine cycle and (ii) a direct contact column (DCC) for flue gas cooling. GTW-CCS adds four more steps to GTW-CONV; namely (i) post-combustion carbon capture via PCC-MEA, removing 90% of flue gas CO_2; (ii) two CO_2 compression units (CO2-CMP#1 and CO2-CMP#2) that compress CO_2 to liquid and pump it via pipelines to EOR in the same oil/gas field; (iii) CO_2 dehydration (located between CO2-CMP#1 and CO2-CMP#2) with triethylene-glycol (TEG unit); and

(iv) a stripping gas unit (STR-CO2) for reducing TEG reboiler temperature. GTW-CCS-EGR adds two intensification layers to GTW-CCS, namely EGR from DCC, and a triple-pressure Rankine cycle.

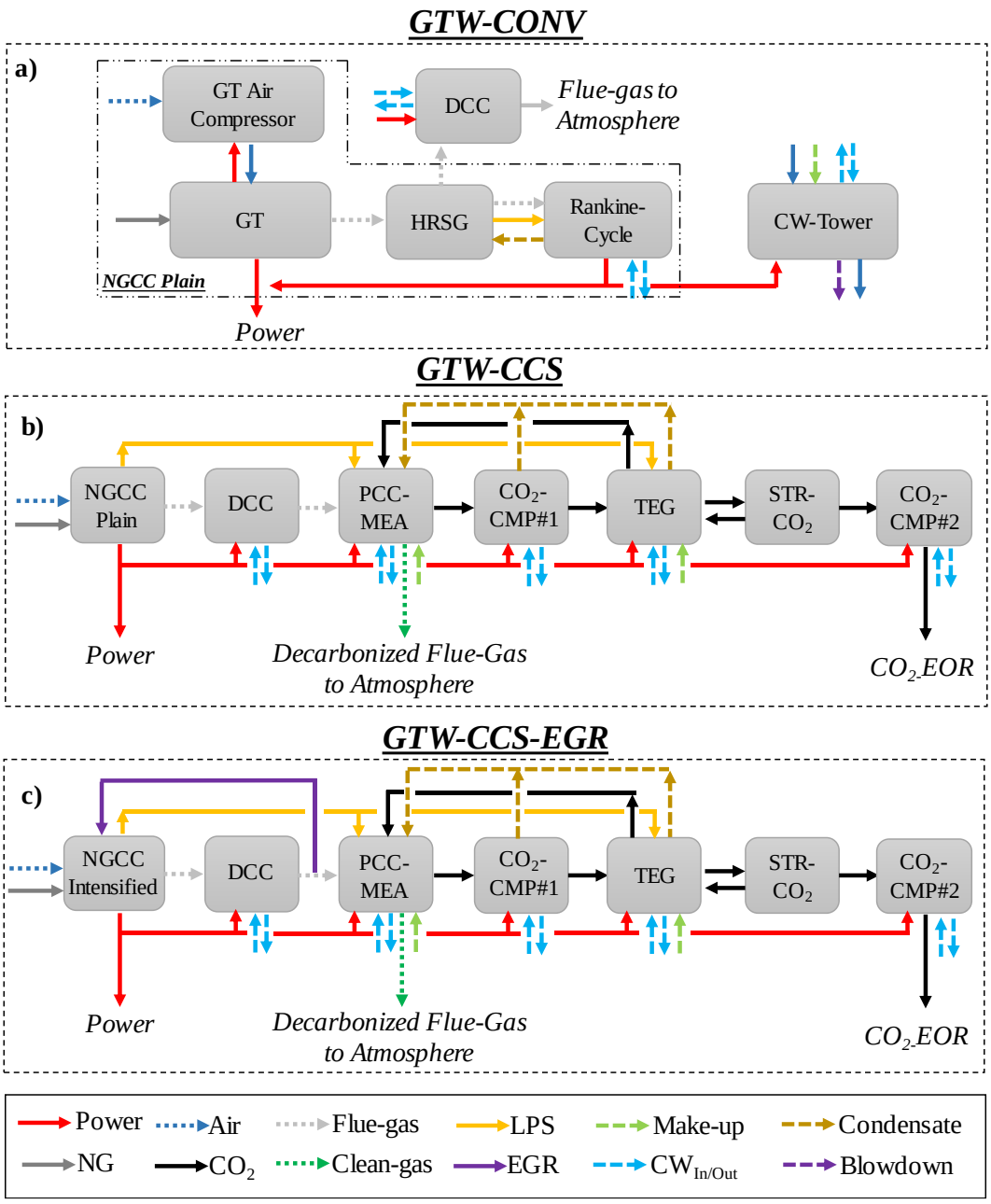

Figure 1. (**a**) GTW-CONV; (**b**) GTW-CCS; and (**c**) GTW-CCS-EGR. (CW: cooling water; GT: gas turbine; TEG: TEG unit).

2.2. Sub-Systems

GTW-CONV, GTW-CCS, and GTW-CCS-EGR were evaluated via simulations in Aspen-HYSYS v10, adopting the assumptions of Table 1a (offshore rig operations) and Table 1b (onshore operations). The Peng–Robinson equation of state (PR-EOS) is used everywhere except for PCC-MEA, TEG unit, and Rankine cycle. Raw CO_2-rich NG is firstly treated in offshore rigs for desulfurization/dehydration, then compressed and sent to an onshore NGCC through pipelines. Pipelines are simulated with the Beggs and Brill model and PR-EOS. Gas turbines are fed with treated 6.5 $MMSm^3/d$ CO_2-rich NG at gas turbine pressure.

Table 1. (a) Design/simulation assumptions of offshore rig operations. (b) Simulation assumptions of onshore operations (CW = cooling water).

(**a**)		
Item	**Description**	**Assumptions**
A1	NG-to-onshore Compressor	Compression Ratio^{Stage} = 1.6; Stages = 4; T^{Intercooler} = 40 °C; P^{Inlet} = 30 bar; P^{Outlet} = 200 bar; T^{Outlet} = 40 °C [43]
A2	Molecular Sieve Temperature Swing Adsorption	P^{Inlet} = 75 bar; Dehydration Target: H_2O = 1 ppm-mol; Adsorption Cycle = 12 h; Regeneration Cycle = 4 h; Mass^{Adsorbent} = 50,000 kg/Vessel; Vessels = 2; Density^{Adsorbent} = 800 kg/m^3; Water^{Adsorbed} = 0.1 kg^{Water}/kg^{Adsorbent} [42];
A3	NG Downcomer	P^{Inlet} = 200 bar; Flexible Pipes = 2; Inner Diameter = 12″; Length = 2000 m; Inclination = −100%; Average T^{External} = 15 °C [45].
A4	NG Pipeline Rig-to-Shore	Inner Diameter = 16″; Max Velocity = 3 m/s; P^{Outlet} $\geq$ 70 bar; Segment-1: Length = 10 km; Inclination = +0.1%; Average T^{External} = 5 °C; Segment-2: Length = 20 km; Inclination = +10%; Average T^{External} = 10 °C; Segment-3: Length = 200 km; Inclination = +0.1%; Average T^{External} = 20 °C [45].
(**b**)		
Item	**Description**	**Assumptions**
A5	Thermodynamic Modeling	Base Model: PR-EOS; PCC-MEA: HYSYS Acid–Gas Package; Pipelines: Beggs and Brill + PR-EOS [45]; CW + Rankine Cycle: HYSYS ASME Steam Table; TEG unit: Glycol Package.
A6	Treated CO_2-Rich NG	6.5 MMm^{3,Std}/d; T = 40 °C; P = 18.5 bar; CO_2 = 44% mol, CH_4 = 50% mol, C_2H_6 = 3% mol, C_3H_8 = 2% mol, C_4H_{10} = 1% mol, H_2O = 1 ppm-mol [49].
A7	CW	T^{Inlet} = 35 °C; T^{Outlet} = 55 °C; P^{Inlet} = 4 bar; P^{Outlet} = 3.5 bar [43].
A8	Adiabatic Efficiencies	η^{Pumps} = 75%; $\eta^{Steam\ Turbine}$ = 85%; $\eta^{\ Compressors}$ = 75%; $\eta^{\ CWT\ Blower}$ = 95%; Gas Turbine: $\eta^{Air\ Compressor}$ = 87%; $\eta^{Expander}$ = 90% [42].
A9	Heat Exchangers	ΔP = 0.5 bar; Thermal Approaches: $\Delta T^{Gas\text{-}CW}$ = 5 °C, $\Delta T^{Gas\text{-}Gas}$ = 10 °C, $\Delta T^{Liq\text{-}Liq}$ = 5 °C [43].
A10	Steam Streams HPS, MPS1, MPS2, LPS (saturated)	GTW-CONV and GTW-CCS: P^{HPS} = 45 bar; T^{HPS} = 545 °C; P^{LPS} = 3 bar; T^{LPS} = 135 °C; GTW-CCS-EGR: P^{HPS} = 90 bar, T^{HPS} = 535 °C; P^{MPS1} = 21 bar, T^{MPS1} = 535 °C; P^{MPS2} = 3.8 bar, T^{MPS2} = 343 °C; P^{LPS} = 4.7 bar, T^{LPS} = 150 °C [45].
A11	HRSG	$\Delta T^{Approach}$ = 50 °C; $\Delta P^{Flue\ Gas}$ = 0.025 bar; ΔP^{Steam} = 0.050 bar [45].
A12	Rankine Cycle	GTW-CONV and GTW-CCS: P^{HPS} = 45 bar; P^{Outlet} = 0.25 bar; Quality^{Outlet} = 95.1%; GTW-CCS-EGR: P^{HPS} = 90 bar; P^{MPS1} = 21 bar; P^{MPS2} = 3.8 bar; P^{Outlet} = 0.16 bar; Quality^{Outlet} = 99.1% [45].
A13	Air	T = 25 °C; P = 1 atm; N_2 = 76.6% mol; O_2 = 20.6% mol; H_2O = 1.9% mol; Ar = 0.9% mol.
A14	Gas Turbine (2 Gas Turbines)	GE9F.05; Air = 170.3 t/h; NG = 3.252 MMsm^3/d; P^{Inlet} = 18 bar; T^{OUT} = 640 °C [50]; GTW-CONV and GTW-CCS: Air = 14.2 kg/kg^{NG}; GTW-CCS-EGR: Air = 6.5 kg/kg^{NG}.
A15	DCC	4-Staged Tray Column; P^{Top} = 1 bar; $T^{Outlet}_{Flue-Gas}$ = 36 °C [42]
A16	PCC-MEA	Solvent: MEA = 29.9% *w*/*w*; H_2O = 70.1% *w*/*w*; Heating Utility: LPS [45]; Absorber: 40-Staged, T$^{Solvent\ Inlet}$ = 36 °C; Stripper: 20-Staged, P^{Condenser} = 1 bar, P^{Reboiler} = 1.3 bar, T$^{Solvent\ Inlet}$ = 90 °C, T^{Condenser} = 40 °C, T^{Reboiler} = 110 °C.
A17	CO_2 Compression	Compression Ratio^{Stage} = 2.7; Stages = 5; T^{Intercooler} = 40 °C [43].
A18	TEG Unit	Lean TEG: TEG = 98.5% *w*/*w*; Absorber: P^{Top} = 46.4 bar, T$^{TEG\ Inlet}$ = 40 °C; Stripper: P^{Condenser} = 1 bar, T$^{TEG\ Inlet}$ = 75 °C, T^{Condenser} = 40 °C, T^{Reboiler} = 140 °C; Absorber = 20-Staged; Stripper = 10-Staged; Dry-CO_2:154 ppm-mol H_2O.
A19	CO_2-to-EOR	P = 300 bar; T = 40 °C; $CO_2^{GTW\text{-}CCS}$ = 99.6% mol; $CO_2^{GTW\text{-}CCS\text{-}EGR}$ = 99.99% mol.
A20	CW Tower	Blowdown = Evaporation; Water$^{Make\text{-}up}$: P = 1.013 bar, T = 30 °C; ΔP^{Blower} = 2 kPa [45].
A21	Steam	Priority: LPS; Surplus: HPS/MPS1/MPS2.
A22	EGR	Flue Gas^{Recycle} = 53.23%; Air^{Inlet}: Stoichiometric.
A23	CO_2 Pipeline Shore-to-Field	P^{Inlet} = 300 bar; P^{Outlet} $\geq$ 750 bar; Inner Diameter = 13″; Max Velocity = 3 m/s; Segment-1: Length = 200 km; Inclination = −0.1%; Average T^{External} = 20 °C; Segment-2: Length = 20 km; Inclination = −10%; Average T^{External} = 10 °C; Segment-3: Length = 10 km; Inclination = −0.1%; Average T^{External} = 5 °C; Segment 4: Length = 3 km; Inclination = −100%; Average T^{External} = 30 °C [45].

2.2.1. NGCC

Figure 2 shows the following NGCC sub-systems: plain (no EGR and a single-pressure Rankine cycle) and intensified (EGR and a triple-pressure Rankine cycle). GTW-CONV and GTW-CCS use an NGCC-Plain, while GTW-CCS-EGR uses an NGCC-Intensified. HRSG preheats CO_2-rich NG at 18 bar to 100 °C. In an NGCC-Plain (Figure 2a), air feeds gas turbines at 14.2 kg^{Air}/kg^{NG}. Two GE Power GE9F.05 gas turbines coupled to electric generators produce constant *Power#1* and flue gas at 640 °C. HRSG cools down the hot flue gas to 150 °C, producing superheated, high-pressure steam (HPS, 45 bar/585 °C), using the HPS condensate from the Rankine cycle condenser. In the steam turbine, HPS expands to 0.25 bar, generating *Power#2*. The HPS condensate (0.25 bar/40 °C) is pumped to 45 bar, consuming *Power#3*. The NGCC-Plain thermodynamic yield reaches 53.7% (*LHV*) without LPS production (GTW-CONV) and 39.14% (*LHV*) with LPS production (GTW-CCS), consuming *Power#4* in the LPS condensate pump. The flue gas from the NGCC-Plain contains 7.21% mol CO_2.

In an NGCC-Intensified (Figure 2b), cold flue gas (36 °C) is recirculated and mixed with stoichiometric air to feed the two gas turbines, which generate constant *Power#1*. HRSG produces LPS (4.7 bar/150 °C)—consuming *Power#4*—and three superheated steams, HPS (90 bar/585 °C), MPS1 (21 bar/585 °C), and MPS2 (3.8 bar/343 °C), for the triple-pressure Rankine cycle [34]. HPS, MPS1, and MPS2 expand to 0.16 bar, generating *Power#2.* in a multi-stage steam turbine. The final MPS2 exhaust is cooled to 40 °C and pumped to 90 bar, 21 bar, and 3.8 bar, consuming *Power#3*. The NGCC-Intensified flue gas contains 15.8% mol CO_2. Due to LPS production, the thermodynamic yield of the NGCC-Intensified reaches 38.61% (*LHV*)—LPS production is 0.2% over-specified above the LPS demand.

2.2.2. Direct Contact Column

Figure 3 shows the flue gas from HRSG being cooled down to 40 °C in the direct contact column (DCC), with cooling water (CW) becoming water saturated. CW is pumped at 35 °C to 4 bar, consuming *Power#5*. The DCC sends hot CW at 55 °C to the CW tower. The water-saturated flue gas is sent to PCC-MEA in GTW-CCS and GTW-CCS-EGR.

2.2.3. PCC-MEA

Flue gas from the DCC feeds the PCC-MEA unit in GTW-CCS and GTW-CCS-EGR. The PCC-MEA, as shown in Figure 4, absorbs CO_2 in the atmospheric 50-staged absorber, fed at the top with lean aqueous MEA (40 °C, 29.9% *w*/*w* MEA). Flue gas is uniformly divided into four inlets, positioned from the bottom to stage 36. The absorber products are water-saturated, decarbonized flue gas, with 0.59% mol CO_2 (GTW-CCS) or 1.37% mol CO_2 (GTW-CCS-EGR) and CO_2-rich solvent at the bottom. The reboiled *20*-staged stripper of PCC-MEA produces atmospheric water-saturated CO_2 (1 atm/40 °C, 92.6% mol CO_2) from the top (total reflux) condenser and lean solvent (T = 110 °C) at the bottom. The absorber's rich solvent is preheated from 52 °C to 90 °C, while the lean solvent is cooled down from 110 °C to 67 °C. Due to LPS production for PCC-MEA, the Rankine cycle net power now corresponds to $Power\#2^{GTW\text{-}CCS}$ and $Power\#2^{GTW\text{-}CCS\text{-}EGR}$, both lower than $Power\#2^{GTW\text{-}CONV}$ (Table 2). PCC-MEA solvent recirculation consumes *Power#6* and the water make-up pump consumes *Power#7*.

2.2.4. CO_2 Compression (CO_2-CMP)

In GTW-CCS and GTW-CCS-EGR, the CO_2 from PCC-MEA is compressed through two intercooled compression trains, as shown in Figure 5. These are a 4-staged CO2-CMP#1, and a single-staged with a pump CO2-CMP#2. After, the fifth compressor CO_2 is a liquid (125 bar/40 °C). It is pumped and cooled down to dispatch conditions (300 bar/40 °C) for the CO_2-to-EOR stream. The carbonated waters from knockout drums return to the first tray of the PCC-MEA stripper, lowering the condenser heat load and avoiding fugitive losses of both CO_2 and water. The compressors and pump consume *Power#8* and *Power#9*, respectively. The water-saturated CO_2 from CO2-CMP#1 is dehydrated in the TEG unit

and STR-CO2 unit. CO2-CMP#2 receives dry CO_2 (≈150 ppm-mol H_2O) and, after a final compression, exports it via the CO_2-to-EOR stream.

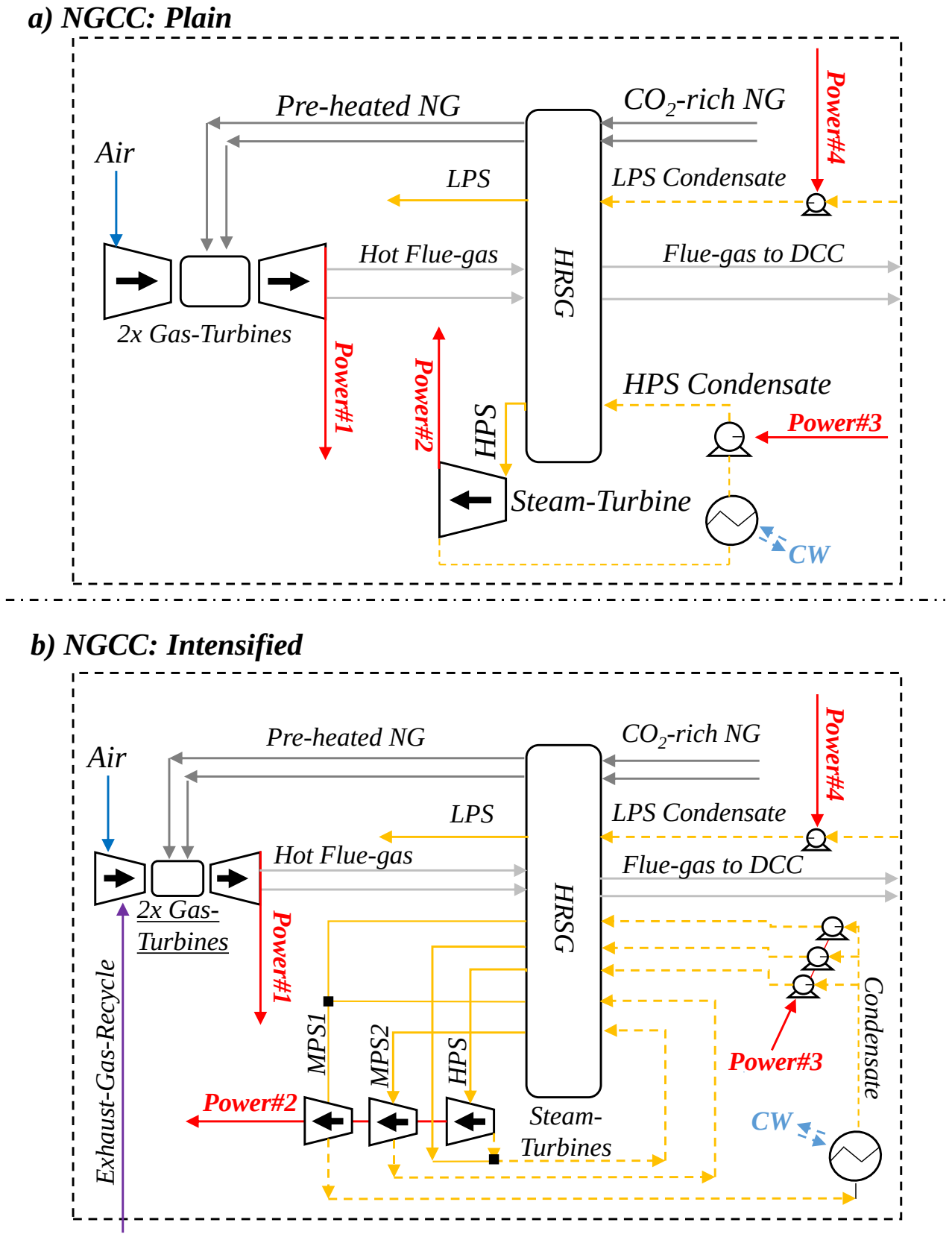

Figure 2. NGCC sub-systems: (**a**) Plain. (**b**) Intensified.

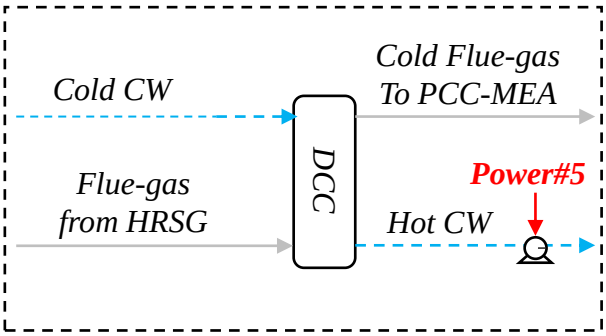

Figure 3. DCC sub-system.

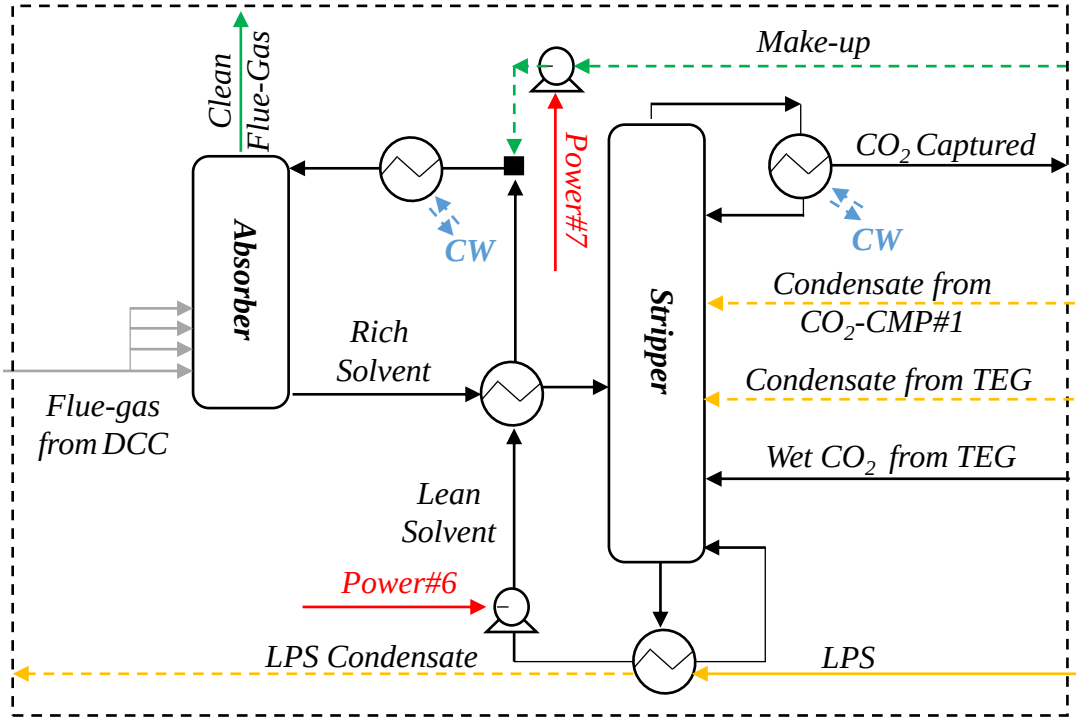

Figure 4. PCC-MEA sub-system.

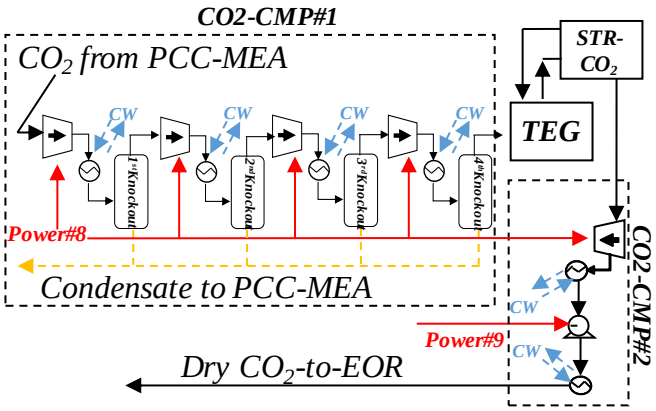

Figure 5. CO_2 compression sub-systems: CO2-CMP#1 and CO2-CMP#2.

Table 2. Power tributaries.

System	Tributaries	Description
Gas Turbines	$Power\#1$	$Power\#1^{GTW\text{-}CCS} > Power\#1^{GTW\text{-}CCS\text{-}EGR}$
Steam Turbines	$Power\#2$	$Power\#2^{GTW\text{-}CONV} > Power\#2^{GTW\text{-}CCS\text{-}EGR} > Power\#2^{GTW\text{-}CCS}$
HPS condensate pump	$Power\#3$	$Power\#3^{GTW\text{-}CONV} > Power\#3^{GTW\text{-}CCS\text{-}EGR} > Power\#3^{GTW\text{-}CCS}$
LPS condensate pump	$Power\#4$	$Power\#4^{GTW\text{-}CCS} > Power\#4^{GTW\text{-}CCS\text{-}EGR}$
DCC pump	$Power\#5$	$Power\#5^{GTW\text{-}CONV} = Power\#5^{GTW\text{-}CCS} = Power\#5^{GTW\text{-}CCS\text{-}EGR}$
PCC-MEA recirculation pump	$Power\#6$	$Power\#6^{GTW\text{-}CCS} > Power\#6^{GTW\text{-}CCS\text{-}EGR}$
PCC-MEA make-up pump	$Power\#7$	$Power\#7^{GTW\text{-}CCS} > Power\#7^{GTW\text{-}CCS\text{-}EGR}$
CO_2 Compressors	$Power\#8$	$Power\#8^{GTW\text{-}CCS} > Power\#8^{GTW\text{-}CCS\text{-}EGR}$
CO_2-to-EOR pump	$Power\#9$	$Power\#9^{GTW\text{-}CCS} \approx Power\#9^{GTW\text{-}CCS\text{-}EGR}$
CW Tower pump	$Power\#10$	$Power\#10^{GTW\text{-}CONV} < Power\#10^{GTW\text{-}CCS} < Power\#10^{GTW\text{-}CCS\text{-}EGR}$
CW Tower make-up pump	$Power\#11$	$Power\#11^{GTW\text{-}CONV} < Power\#11^{GTW\text{-}CCS} < Power\#1^{GTW\text{-}CCS\text{-}EGR}$
CW Tower blower	$Power\#12$	$Power\#1^{GTW\text{-}CONV} < Power\#12^{GTW\text{-}CCS} < Power\#6^{GTW\text{-}CCS\text{-}EGR}$
TEG pump	$Power\#13$	-
TEG make-up pump	$Power\#14$	-
CW Tower GTW-CONV	$PowerCWT^{GTW\text{-}CONV}$	$Power\#10 + Power\#11 + Power\#12$
CW Tower GTW-CCS	$PowerCWT^{GTW\text{-}CCS}$	$Power\#10 + Power\#11 + Power\#12$
CW Tower GTW-CCS-EGR	$PowerCWT^{GTW\text{-}CCS\text{-}EGR}$	$Power\#10 + Power\#11 + Power\#12$
PCC-MEA	$Power^{PCC\text{-}MEA}$	$Power\#6 + Power\#7$
CO_2-CMP	$Power^{CO2\text{-}CMP}$	$Power\#8 + Power\#9$
GTW-CONV	$Power^{GTW\text{-}CONV}$	$Power\#1 + Power\#2 - Power\#3 - Power\#5 - PowerCWT^{GTW\text{-}CONV}$
GTW-CCS	$Power^{GTW\text{-}CCS}$	$Power\#1 + Power\#2 - Power\#3\text{-}Power\#4 - Power\#5 - Power^{PCC\text{-}MEA} - Power\#^{CO2\text{-}CMP} - PowerCWT^{GTW\text{-}CCS}$
GTW-CCS-EGR	$Power^{GTW\text{-}CCS\text{-}EGR}$	$Power\#1 + Power\#2 - Power\#3 - Power\#4 - Power\#5 - Power^{PCC\text{-}MEA} - Power\#^{CO2\text{-}CMP} - PowerCWT^{GTW\text{-}CCS\text{-}EGR} - Power\#13 - Power\#14$

2.2.5. TEG Dehydration Unit (TEG) and Stripping CO_2 Unit (STR-CO_2)

Water-saturated CO_2 (≈1400 ppm-mol H_2O, 46 bar/40 °C) from CO2-CMP#1 is dehydrated by the TEG unit (Figure 6). The 20-staged absorber with 98.5% *w*/*w TEG* produces dry CO_2 (≈150 ppm-mol H_2O) at the top and water-rich solvent at the bottom. The solvent is recovered in the reboilered, 10-staged TEG stripper, which produces atmospheric water-saturated CO_2 (1 atm/40 °C, 92.6% mol CO_2) plus aqueous distillate in the partial condenser, as well as lean TEG at the bottom (T = 140 °C). A heat integration exchanger preheats the rich TEG from 37 °C to 75 °C, while cooling down the lean TEG from 140 °C to 70 °C. The STR-CO2 unit expands a small fraction (≈0.63%) of dry CO_2 from the absorber to the TEG reboiler pressure and also feeds a countercurrent exchanger to cool down the remaining dry CO_2. This expanded gas is injected as stripping gas to maintain the reboiler at 140 °C, minimizing TEG degradation. TEG losses are compensated by make-up TEG (98.5% *w*/*w*), consuming *Power#14* in the make-up pump. The TEG recirculation pump consumes *Power#13*.

2.2.6. Cooling Water Tower

The CW tower (Figure 7) regenerates cold CW from hot CW. Blowdown and evaporation represent losses that are compensated by water make-up. Evaporation and blowdown flow rates are assumed equal (Table 1b). *Power#10* (CW pump), *Power#11* (make-up pump), and *Power#12* (fan) are lower in GTW-CONV, relative to GTW-CCS and GTW-CCS-EGR, due to a lower GTW-CONV CW demand. Table 2 shows the power tributaries of GTW-CONV, GTW-CCS, and GTW-CCS-EGR.

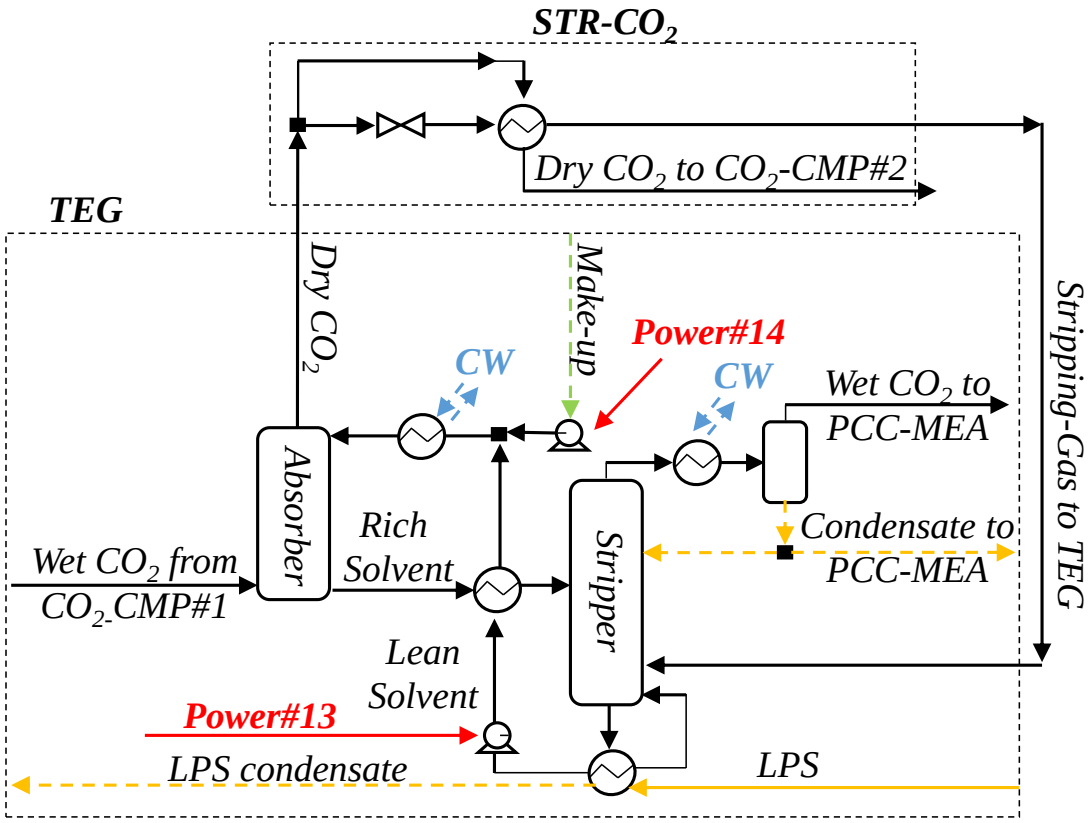

Figure 6. TEG dehydration unit and STR-CO_2 unit.

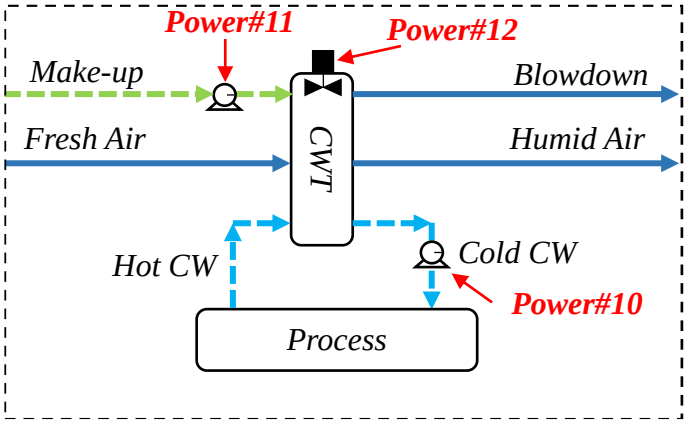

Figure 7. CW tower (CWT).

2.3. Economic Analysis

Economic analysis follows that of Turton et al. [51] for estimating equipment-fixed capital investment (*FCI*, *MMUSD*), in both onshore and offshore operations; the annual cost of manufacturing (*COM*, *MMUSD*/*y*); and net present value (*NPV*, *MMUSD*), using Equations (1a)–(1c) and (2)–(6) after process design and sizing. It should be noticed that the present economic evaluation is centered on the *NPV*, *COM*, and *FCI* metrics, but other metrics could also be used like the internal rate of return (*IRR*). In spite of the obvious differences between *IRR* and *NPV*, in general, it is expected that the use of *IRR* would not bring different conclusions in the economic comparison of alternatives as carried out here using *NPV*, *COM*, and *FCI* [51].

Note that the *FCI* of offshore operations is assumed to be higher via Equation (1b), and *NEQ* represents the number of items of equipment. The bare module costs (C_{BM})

are calculated from the costs of purchase in a condition of reference, corrected via factors taking into account the design, material, and pressure, as well as being updated via the annual average Chemical Engineering Plant Cost Index (CEPCI) of 816.0 for 2022 [52]. For equipment items with a capacity factor (*CF*) beyond the correlation capacity factor limits, C_{BM} is estimated via the Six-Tenth Rule (Equation (2)). The economic assumptions in Table 3 are necessary for estimating economic variables like (i) revenues from electricity and CO_2-to-EOR (*REV*, *MMUSD*/*y*); (ii) raw material costs (*CRM*, *MMUSD*/*y*) that derive from make-up (water, TEG and MEA), molecular-sieve reposition (TSA in offshore operations), and NG intake; (iii) labor cost (*COL*, *MMUSD*/*y*); (iv) annual depreciation (*DEPR*, *MMUSD*/*y*); and (v) gross annual profit (*GAP*, *MMUSD*/*y*) and annual profit (*AP*, *MMUSD*/*y*). The utility cost (electricity + CW) is zero because the plant produces its own electricity and CW (*CUT* = 0 *MMUSD/y*). *NPV* is given by Equation (6), where *N* and *i* (%) represent the number of operational years and the annual interest rate. The *FCI* of NG and CO_2 pipelines was estimated based on Carminati et al. [53], who used topographic data in the pre-salt basin, consisting of four segments from shore-to-field (or in reversed order from field-to-shore), as follows: (i) Segment 1: continental shelf (200 km, −0.1% inclination); (ii) Segment 2: continental slope (20 km, −10% inclination); (iii) Segment 3: submarine plateau (10 km, −0.1% inclination); and (iv) Segment 4: CO_2 injection column (3 km, −100% inclination). The NG downcomer (2 km, −100% inclination) comprehends two flexible ducts, transporting compressed NG from the rig to the submarine pipeline.

$$FCI^{Onshore} = 1.18 \times \sum_{j=1}^{NEQ} C_{BM}(j) \quad \{Onshore\ Operations \tag{1a}$$

$$\begin{cases} FCI^{Offshore}(k)/FCI^{Onshore}(k) = 2.00 \\ FCI^{Offshore} = \sum_{k=1}^{NEQ} FCI^{Offshore}(k) \end{cases} \quad \{Offshore\ Operations \tag{1b}$$

$$FCI = FCI^{Onshore} + FCI^{Offshore} \tag{1c}$$

$$C_{BM}(j) = C_{BM}^{Lim}(j) \times \left(\left(CF(j)/CF^{Lim}(j)\right)\right)^{0.6} \tag{2}$$

$$CRM = CRM^{Water} + CRM^{TEG} + CRM^{MEA} + CRM^{Molecular-Sieve} + CRM^{NG} \tag{3}$$

$$COM = (1.23 \times CUT) + (1.23 \times CRM) + (2.73 \times COL) + (0.18FCI) \tag{4}$$

$$AP = \begin{cases} GAP - ((GAP - DEPR) \times (ITR \times 0.01)), if\ (GAP > DEPR) \\ GAP,\ if(GAP \leq DEPR) \\ where, GAP = REV - COM \end{cases} \tag{5}$$

$$NPV = AP \times \left(\sum_{k=2}^{N+2} q^{-k}\right) - \left(\left(0.40 + 0.60 \times q^{-1}\right) \times FCI\right), \quad q = (1 + i/100) \tag{6}$$

Table 3. Assumptions for economic analysis.

Item	Parameter	Assumption
E1	Operation lifetime (y)	30
E2	Construction time (y)	2 (40%/60%)
E3	Operation (h/y)	8400
E4	*i* (%)	10
E5	*DEPR* (%FCI)	10
E6	*ITR* (%)	34
E7	NG price (USD/MMBTU) [54]	2.82
E8	Electricity price (USD/kWh) [55]	0.1026
E11	Labor cost (USD/y.operator) [51]	89,100
E12	EOR yield (bbl^{Oil}/t^{CO2}) [56]	1.5
E13	*MEA* Price (USD/kg)	2

Table 3. *Cont.*

Item	Parameter	Assumption
E14	Water Make-up Price (USD/m^3) [45]	0.0003
E15	*FCI* CW Tower (USD/GPM) [57]	40
E16	Molecular Sieve (USD/kg)	1.0
E17	NG Downcomer	4 MMUSD/km
E18	NG Pipeline (Segment 1) [53]	4 MMUSD/km
E19	NG Pipeline (Segment 2) [53]	4 MMUSD/km
E20	NG Pipeline (Segment 3) [53]	3 MMUSD/km
E21	CO_2 Pipeline (Segment 1) [53]	2 MMUSD/km
E22	CO_2 Pipeline (Segment 2) [53]	3 MMUSD/km
E23	CO_2 Pipeline (Segment 3) [53]	3 MMUSD/km
E24	CO_2 Pipeline (Segment 4) [53]	3 MMUSD/km

2.4. Multi-Criteria Sustainability Analysis

Sustainability is multi-dimensional, comprehending at least the environment, as well as both social and economic dimensions. Hence, assessing sustainability performance requires managing multiple metrics with uncertainties and regional dependences, i.e., a multi-criteria analysis is necessary. There are several approaches to assess sustainability, e.g., multi-criteria analysis, life-cycle costing, and life-cycle analysis (LCA). LCA performs a "cradle-to-gate" analysis, assessing the impacts of the production chain and product utilization. GREENSCOPE [58] uses 139 indicators to assess process sustainability (i.e., a "gate-to-gate" analysis). It proposes the best- and worst-case scenarios as the upper bounds and lower bounds of each indicator. These bounds are used to normalize indicators from 0% to 100%. The global dimension score is calculated by averaging the indicator scores belonging to that dimension. For example, the energy dimension global score is the arithmetic mean of the *Eeff*, *Ecp*, *ER*, and *EU* scores. In a similar way, global scores are computed for the economic, environmental, and material dimensions. Consequently, each process alternative—GTW-CONV, GTW-CCS, GTW-CCS-EGR—presents global scores for these four dimensions. Table 4 shows a selection of 17 GREENSCOPE indicators to assess the sustainability of GTW-CONV, GTW-CCS, and GTW-CCS-EGR. The best and worst cases follow from [58].

Table 4. GREENSCOPE indicators for sustainability performance.

Symbol	Definition	Unit	Best Case	Worst Case
Economic				
NPV	Net Present Value	USD	0% interest	*NPV* = 0
DPBP	Discounted Payback Periodfor *NPV* = 0	y	*DPBP* = 3	*DPBP* = 30
TR	Turnover Ratio (Revenues/*FCI*)	USD/USD	*TR* = 4	*TR* = 0
COM	Cost of Manufacture	USD/y	*COM* = 0	*COM* = Revenues
CRMv	Cost of Raw Material per Power Exported (Hourly)	USD/kWh	*CRMv* = 0	Revenues/Power Exported
Environmental				
HS	No. of Hazardous Substance Inputs	-	*HS* = 0	All inputs hazardous
HSs	Hazardous Substances Consumption per Power Exported	kg/kWh	*HSs* = 0	All inputs hazardous
CI	CO_2 Emitted per Power Exported	kg/kWh	*CI* = 0	100% CO_2 emitted
CIv	CO_2 Emitted per Revenues	kg/USD	*CIv* = 0	100% CO_2 emitted
Material				
Mcp	Mass Input	kg	Equals $Mass^{Output}$	40 * $Mass^{Output}$
MI	Mass Consumption per Power Exported	kg/kWh	1	40
WI	Water Consumption per Power Exported	m^3/kWh	0	*MI* = *WI*
WIv	Water Consumption per Revenues	m^3/USD	0	1.55
Energy				
Eff	Power Produced per Energy Input	kW/kW	1	0
Ecp	Energy Consumption	kW	0	Power Produced
ER	Power Demand per Power Exported	kW/kW	0	1
EU	Energy Required by Utilities	kW	0	10% of Power Exported

2.5. Thermodynamic Analysis of Processes

Thermodynamic analysis is applied to GTW-CONV, GTW-CCS, and GTW-CCS-EGR and their sub-systems. As defined by the light shed by the second law of thermodynamics, any open-system operating at steady-state is either a power-producing system or a power-consuming system. Power-producing systems conduct spontaneous processes (e.g., NGCC and DCC), while power-consuming systems conduct non-spontaneous processes (e.g., separation processes like PCC-MEA). Figure 8 depicts a typical open system operating at steady-state with multiple feed streams and product streams. The open system can only have thermal interactions with an isothermal heat reservoir (R_0) maintained at temperature T_0 (T_0 = 298.15 K). The open system can import power ($\dot{W} < 0$) or export power ($\dot{W} > 0$), but it only thermally interacts with R_0, rejecting heat ($\dot{Q} < 0$) or absorbing heat ($\dot{Q} > 0$). $F_n, \overline{H}_{F_n}, \overline{S}_{F_n}$, respectively, represent the flow rate (kmol/s), enthalpy (MJ/kmol), and entropy (MJ/kmol.K) of the nth feed-stream, while $K_n, \overline{H}_{K_n}, \overline{S}_{K_n}$ are analogues for the nth product stream.

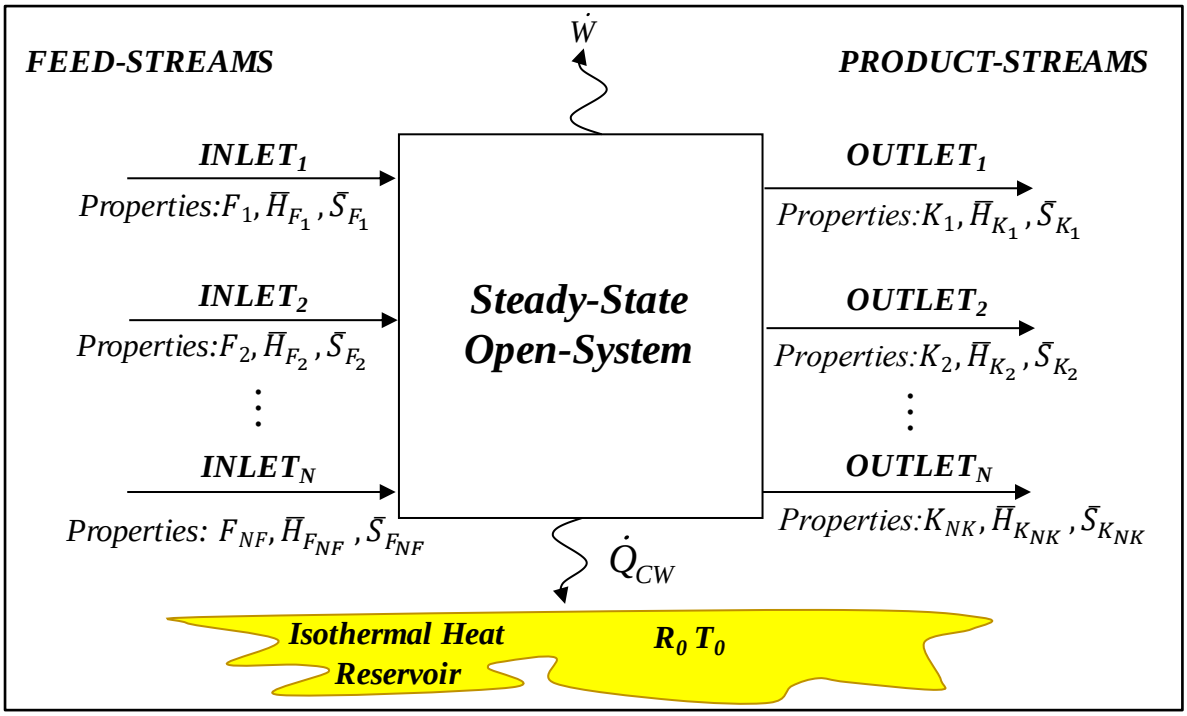

Figure 8. Open system operating at steady-state with heat reservoir R_0 at T_0.

2.5.1. Maximum Work

The first law of thermodynamics is applied to the steady-state open system represented in Figure 8, resulting in Equations (7) and (8). The maximum work (power), $\dot{W}^{MAX}$, is obtained via Equations (9)–(11) at reversible conditions, where $\dot{S}^{Univ}$ is the rate of the entropy creation of the Universe, due to the open system. At reversibility, Equation (10) expresses $\dot{S}^{Univ}$, wherein its last term on the right represents the entropy rate of $\boldsymbol{R_0}$. Equation (11) results from Equation (8) under reversibility, where $\dot{Q}^{REV}$ is isolated in Equation (12) from Equation (10). Equation (13) or Equation (14) gives $\dot{W}^{MAX}$, after substituting Equation (12) into Equation (8). $\dot{W}^{MAX}$ is positive for power-producing systems (i.e., systems that evolve spontaneously and, consequently, can produce power) and negative for power-consuming systems (i.e., non-spontaneous systems that only evolve impelled by external power).

$$\sum_{i=1}^{NF} F_i \overline{H}_{F_i} + \dot{Q} - \dot{W} = \sum_{i=1}^{NK} K_i \overline{H}_{K_i} \quad (7)$$

$$\dot{W} = -\left(\sum_{i=1}^{NK} K_i \overline{H}_{K_i} - \sum_{i=1}^{NF} F_i \overline{H}_{F_i} \right) + \dot{Q} \quad (8)$$

$$\dot{W} = \dot{W}^{MAX}, \ \dot{Q} = \dot{Q}^{REV}; \ \dot{S}^{UNIV} = 0 \quad (9)$$

$$\dot{S}^{UNIV} = \sum_{i=1}^{NK} K_i \overline{S}_{K_i} - \sum_{i=1}^{NF} F_i \overline{S}_{F_i} - \frac{\dot{Q}^{REV}}{T_0} = 0 \quad (10)$$

$$\dot{W}^{MAX} = -\left(\sum_{i=1}^{NK} K_i \overline{H}_{K_i} - \sum_{i=1}^{NF} F_i \overline{H}_{F_i} \right) + \dot{Q}^{REV} \quad (11)$$

$$\dot{Q}^{REV} = T_0 \left\{ \sum_{i=1}^{NK} K_i \overline{S}_{K_i} - \sum_{i=1}^{NF} F_i \overline{S}_{F_i} \right\} \quad (12)$$

$$\dot{W}^{MAX} = -\left(\sum_{i=1}^{NK} K_i \overline{H}_{K_i} - \sum_{i=1}^{NF} F_i \overline{H}_{F_i} \right) + T_0 \left\{ \sum_{i=1}^{NK} K_i \overline{S}_{K_i} - \sum_{i=1}^{NF} F_i \overline{S}_{F_i} \right\} \quad (13)$$

$$\dot{W}^{MAX} = -\left(\sum_{i=1}^{NK} K_i (\overline{H}_{K_i} - T_0 \overline{S}_{K_i}) - \sum_{i=1}^{NF} F_i (\overline{H}_{F_i} - T_0 \overline{S}_{F_i}) \right) \quad (14)$$

2.5.2. Equivalent Power

Equivalent power comprehends all system power effects, including electricity $\dot{EE}$ (MW) produced ($\dot{EE}^{PROD}$) or consumed ($\dot{EE}^{CONS}$), and equivalent power effects from system interactions with utilities. Gas-to-wire uses two utilities, (i) cooling water (CW): flow rate F^{CW} (kmol/s), isobaric molar heat capacity $\overline{C}_P{}^{CW}$ (MJ/kmol.K), hot temperature T_H^{CW} (K), and cold temperature T_C^{CW} (K); (ii) saturated steam (SS): flow rate F^{SS} (kmol/s), molar enthalpy of vaporization $\Delta\overline{H}_{SS}^{VAP}$ (MJ/kmol), and temperature T^{SS} (K). GTW-CCS and GTW-CCS-EGR adopt SS as LPS. $\overline{C}_P{}^{CW}$ and $\Delta\overline{H}_{SS}^{VAP}$ are supposed to be constant, as a consequence of the narrow temperature ranges in which CW and LPS operate.

The concept of equivalent power not only comprehends true power streams ($\dot{EE}^{CONS}$ and $\dot{EE}^{PROD}$), but also incorporates the potential power effects associated with the consumption of utilities by the system. These potential power effects (or equivalent power) are established exclusively using the reversible Carnot engine (CE) and the reversible Carnot heat pump (CHP), in order to achieve maximum yield in heat work conversion [29]. A CE takes heat from a hot source, releases heat to a colder one, and consequently exports power. On the other hand, a CHP takes heat from a cold source, liberates heat to a hotter one, and consequently imports power. Figure 9a shows a power-consuming open system continuously consuming electricity $\dot{EE}^{CONS}$ and rejecting heat $\dot{Q}_{CW}$ to CW (generating hot CW), which is equivalent to a CW loop wherein power $\dot{W}_{CW}^{Eq}$ is continuously exported through CE. Similarly, Figure 9b represents a power-consuming open system continuously consuming electricity $\dot{EE}^{CONS}$ and absorbing heat $\dot{Q}_{SS}$ from SS (generating SS condensate), which is equivalent to an SS loop wherein power $\dot{W}_{SS}^{Eq}$ is continuously imported through CHP. A CW loop and an SS loop do not cross the boundaries of the system, while CE and CHP are attached to R_0, which is always a cold sink. $\dot{W}_{CW}^{Eq}$, $\dot{Q}_{CW}$, $\dot{W}_{SS}^{Eq}$, and $\dot{Q}_{SS}$ must be interpreted as positive numbers. In Figure 9a, the open system loses heat $\dot{Q}_{CW}$ to cold CW, which becomes hot CW. Then, CE absorbs $\dot{Q}_{CW}$, restoring cold CW, while exporting power $\dot{W}_{CW}^{Eq}$ and rejecting heat $\dot{Q}^{R_0}{}_{CW}$ to R_0. In Figure 9b, the open system takes heat $\dot{Q}_{SS}$

from SS, condensing it. Then, CHP supplies $\dot{Q}_{SS}$ to the SS condensate, restoring SS, while importing power $\dot{W}_{SS}^{Eq}$ and absorbing heat $\dot{Q}^{R_0}{}_{SS}$ from R_0. $\dot{W}_{CW}^{Eq}$ and $\dot{W}_{SS}^{Eq}$ are determined via Carnot relationships for CE/CHP processes, as given in Equations (15) and (17), the latter standing for CE/CHP entropy conservation, while Equation (16) defines the heat effects of CW and SS. Substituting Equation (16) and Equation (17) into Equation (15), one obtains Equation (18) for $\dot{W}_{CW}^{Eq}$ and $\dot{W}_{SS}^{Eq}$.

$$\dot{W}_{CW}^{Eq} = \dot{Q}_{CW} - \dot{Q}_{CW}^{R_0};\ \dot{W}_{SS}^{Eq} = \dot{Q}_{SS} - \dot{Q}_{SS}^{R_0} \tag{15}$$

$$\dot{Q}_{CW} = F^{CW}\overline{C}_P^{CW}(T_H^{CW} - T_C^{CW});\ \dot{Q}_{SS} = F^{SS}\Delta\overline{H}_{SS}^{VAP} \tag{16}$$

$$\frac{\dot{Q}_{CW}^{R_0}}{T_0} + F^{CW}\overline{C}_P^{CW} ln\left(\frac{T_C^{CW}}{T_H^{CW}}\right) = 0; -\frac{\dot{Q}_{SS}^{R_0}}{T_0} + F^{SS}\frac{\Delta\overline{H}_{SS}^{VAP}}{T^{SS}} = 0 \tag{17}$$

$$\dot{W}_{CW}^{Eq} = F^{CW}\overline{C}_P^{CW}\left(T_H^{CW} - T_C^{CW} - T_0.ln\left(\frac{T_H^{CW}}{T_C^{CW}}\right)\right);\ \dot{W}_{SS}^{Eq} = F^{SS}\Delta\overline{H}_{SS}^{VAP}\left(1 - \frac{T_0}{T^{SS}}\right) \tag{18}$$

For power-consuming systems—e.g., separation and compression processes like PCC-MEA, TEG units, and CO_2 compression—with electricity consumption $\dot{EE}^{CONS}$, as well as CW consumption and SS (LPS) consumption, the total equivalent power consumed by the system is given by Equation (19a). Alternatively, for power-producing systems (e.g., NGCC, DCC, and CW tower) with electricity production $\dot{EE}^{PROD}$, as well as SS (LPS) production and CW consumption, the total equivalent power produced by the system is given by Equation (19b). Equation (18) is substituted into Equations (19a) and (19b), giving the equivalent power in Equation (20a) for power-consuming systems and in Equation (20b) for power-producing systems.

$$\dot{W}^{Eq} = \dot{EE}^{CONS} + \dot{W}_{SS}^{Eq} - \dot{W}_{CW}^{Eq}\ \{power - consuming\ system \tag{19a}$$

$$\dot{W}^{Eq} = \dot{EE}^{PROD} + \dot{W}_{SS}^{Eq} + \dot{W}_{CW}^{Eq}\ \{power - producing\ system \tag{19b}$$

$$\dot{W}^{Eq} = \dot{EE}^{CONS} + F^{SS}\Delta\overline{H}_{SS}^{VAP}\left(1 - \frac{T_0}{T^{SS}}\right) - F^{CW}\overline{C}p^{CW}\left(T_H^{CW} - T_C^{CW} - T_0.ln\left(\frac{T_H^{CW}}{T_C^{CW}}\right)\right) \tag{20a}$$

$$\dot{W}^{Eq} = \dot{EE}^{PROD} + F^{SS}\Delta\overline{H}_{SS}^{VAP}\left(1 - \frac{T_0}{T^{SS}}\right) + F^{CW}\overline{C}p^{CW}\left(T_H^{CW} - T_C^{CW} - T_0.ln\left(\frac{T_H^{CW}}{T_C^{CW}}\right)\right) \tag{20b}$$

2.5.3. Thermodynamic Efficiency

The thermodynamic efficiency of open systems is determined through second law analysis. With $\dot{W}^{MAX}$ and $\dot{W}^{Eq}$ for power-producing systems and power-consuming systems, thermodynamic efficiencies are calculated through Equation (21a) for power-consuming systems and through Equation (21b) for power-producing systems. It is important to note that $\dot{W}^{Eq}$ has no algebraic sign a priori—but it may become negative for a power-producing system with $\dot{EE}^{PROD} < 0$ (e.g., DCC)—while $\dot{W}^{MAX}$ always follows the work sign convention of thermodynamics.

$$\eta\% = 100.\ (-\dot{W}^{MAX})/\dot{W}^{Eq} \tag{21a}$$

$$\eta\% = 100.\dot{W}^{Eq}/\dot{W}^{MAX} \tag{21b}$$

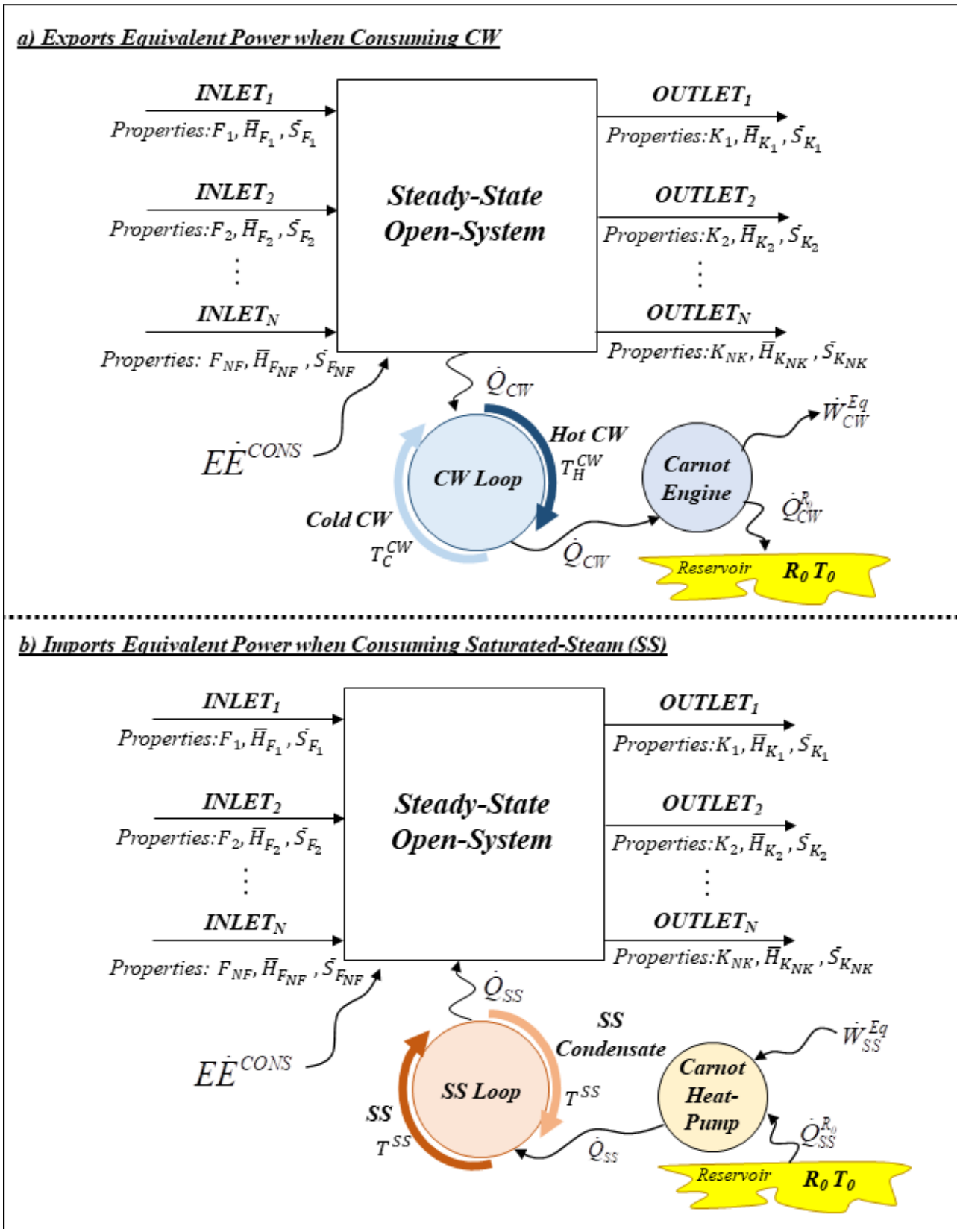

Figure 9. Power-consuming system operation. (**a**) Exports equivalent power through Carnot engine and CW loop (CW consumption). (**b**) Imports equivalent power through Carnot heat pump and SS loop (SS consumption).

2.5.4. Lost Work

Lost work is calculated though $\dot{W}^{MAX}$ and $\dot{W}^{Eq}$ via Equation (22a) for power-consuming systems and via Equation (22b) for power-producing systems.

$$\dot{W}^{LOST} = \dot{W}^{Eq} - (-)\dot{W}^{MAX} \tag{22a}$$

$$\dot{W}^{LOST} = \dot{W}^{MAX} - \dot{W}^{Eq} \tag{22b}$$

It can be demonstrated that alternative lost work formulas—represented by Equation (23b) for power-consuming and by Equation (23c) for power-producing systems—emerge from the well-known second law formula, Equation (23a), that takes into account all changes in the Universe as consequences of system operations [29]. It is worth mentioning that the first two terms on the right-hand side of Equations (23b) and (23c) represent the rate of the entropy change of R_0 multiplied by T_0.

$$\dot{W}^{LOST} = T_0 \dot{S}^{UNIV} \tag{23a}$$

$$\dot{W}^{LOST} = -F^{SS}\Delta\overline{H}_{SS}^{VAP}\left(\frac{T_0}{T^{SS}}\right) + F^{CW}\overline{C}p^{CW}T_0.ln\left(\frac{T_H^{CW}}{T_C^{CW}}\right) + T_0\left(\sum_{i=1}^{NK} K_i\overline{S}_{K_i} - \sum_{i=1}^{NF} F_i\overline{S}_{F_i}\right) \tag{23b}$$

$$\dot{W}^{LOST} = F^{SS}\Delta\overline{H}_{SS}^{VAP}\left(\frac{T_0}{T^{SS}}\right) + F^{CW}\overline{C}p^{CW}T_0.ln\left(\frac{T_H^{CW}}{T_C^{CW}}\right) + T_0\left(\sum_{i=1}^{NK} K_i\overline{S}_{K_i} - \sum_{i=1}^{NF} F_i\overline{S}_{F_i}\right) \tag{23c}$$

3. Results and Discussion

The techno-economic and thermodynamic analysis results are discussed. Simulation results were obtained with Aspen-HYSYS v10 [59].

3.1. Technical Results

NGCC-Plain and NGCC-Intensified consume 6.5 $MMm^{3,Std}$/d of CO_2-rich NG and produce different powers through gas turbines and steam turbines in GTW-CONV, GTW-CCS, and GTW-CCS-EGR. Tables 5 and 6, respectively, show the main streams, the power effects, and utilities consumed/produced in GTW-CONV, GTW-CCS, and GTW-CCS-EGR. Table 6 shows that for GTW-CONV the power demand, power produced, and power exported are, respectively, [10.51 MW, 873.89 MW, 863.38 MW]. For GTW-CCS and GTW-CCS-EGR, the respective analogues are [74.38 MW, 636.86 MW, 562.48 MW] and [74.71 MW, 628.27 MW, 553.56 MW]. GTW-CCS and GTW-CCS-EGR generate less (≈26%) electricity, a consequence of their inferior Rankine cycle performances due to lower HPS production, on behalf of LPS consumed (1278 t/h and 1260.45 t/h, respectively) by PCC-MEA stripper. Additionally, GTW-CCS and GTW-CCS-EGR also have a ≈611% greater power demand, spent with circulation pumps (PCC-MEA, TEG unit) and CO_2 compression units CO2-CMP#1 and CO2-CMP#2. These capture and pump/compression penalties compose the CCS energy penalties of GTW-CCS and GTW-CCS-EGR, which, in terms of loss of exported power, totalize, respectively, 34.9% and 35.9%. For LPS production, the GTW-CCS Rankine cycle has an HPS loss (96.4%), while GTW-CCS-EGR has a lower HPS loss (90.50%) due to triple-pressure Rankine cycle intensification. EGR intensification imposes a lower gas turbine power output in GTW-CCS-EGR—from 628 MW to 604.91 MW—for the same NG flow rate. This 1.4% loss of gas turbine *LHV* efficiency derives from a reduced gas turbines flue gas flow rate, since the EGR flue gas has a higher heat capacity due to higher CO_2/H_2O contents, i.e., for the same exhaust temperature (640 °C, Table 1), less flue gas expands in the gas turbine with EGR. This overshadows the advantage of a lower EGR air compression power, i.e., the net EGR gas turbines' output is lower. CO_2 compression/pumping power consumptions are equal for GTW-CCS (63.45 MW) and GTW-CCS-EGR (63.50 MW). Since CCS imposes extra heating/power, it imposes higher CW consumption. Thus, CW tower

power consumptions of GTW-CONV, GTW-CCS, and GTW-CCS-EGR are, respectively, 7.67 MW, 8.79 MW, and 9.02 MW.

Table 5. Main streams of GTW-CONV, GTW-CCS, and GTW-CCS-EGR.

Case		GTW-CONV	GTW-CCS		GTW-CCS-EGR		
Stream	**NG Feed**	**Flue Gas**	**Clean Flue Gas**	**CO_2-to-EOR**	**Flue Gas to PCC-MEA**	**Clean Flue Gas**	**CO_2-to-EOR**
T (°C)	40	40	55	40	36.5	62.9	40
P (bar)	18.5	1 atm	1 atm	300	1.05	1 atm	300
Flow rate (kmol/h)	11,459.8	181,869.1	176,135.0	11,623.3	79,530.5	78,143.2	11,496.1
CH_4 (% mol)	50	0	0	0	0	0	0
C_2^+ (% mol)	6	0	0	0	0	0	0
CO_2 (% mol)	44	7.21	0.59	99.64	15.80	1.37	99.95
H_2O (% mol)	≈0	5.89	13.98	0.33	6.08	20.0	0.03
N_2 (% mol)	0	74.36	73.86	0.03	77.22	78.6	0.02
O_2 (% mol)	0	11.65	11.57	0	0	0	0
H_2 (% mol)	0	0	0	0	0	0	0
Ar (% mol)	0	0.89	0	0	0.90	0	0

Table 6. Power/utilities of GTW-CONV, GTW-CCS, and GTW-CCS-EGR.

		Consumption/Production		
		GTW-CONV	**GTW-CCS**	**GTW-CCS-EGR**
Tributaries			**Power (MW)**	
Gas Turbine	*Power#1*	628.00	628.00	604.91
Steam Turbines	*Power#2*	245.89	8.86	23.36
HPS Condensate Pump	*Power#3*	1.44	0.05	0.26
LPS Condensate Pump	*Power#4*	-	0.03	0.01
DCC Pump	*Power#5*	1.40	1.40	1.40
PCC-MEA Recirculation Pump	*Power#6*	-	0.56	0.53
PCC-MEA Make-up Pump	*Power#7*	-	0.03	0.02
CO_2 Compressors	*Power#8*	-	58.70	58.64
CO_2-to-EOR Pump	*Power#9*	-	4.80	4.81
CW Tower Pump	*Power#10*	3.81	4.35	4.45
CW Tower Make-up Pump	*Power#11*	0.23	0.25	0.29
CW Tower Fan	*Power#12*	3.63	4.19	4.28
TEG Recirculation Pump	*Power#13*	-	0.01	0.01
TEG Make-up Pump	*Power#14*	-	0.01	0.01
Power Generated		873.89	636.86	628.27
Power Demand		10.51	74.38	74.71
Net Power Exported		863.38	562.48	553.56
Utilities (t/h)				
LPS		-	1278.2	1260.45
CW		35,424.0	41,715.9	42,679.0

Table 7 shows the PCC-MEA results for GTW-CCS and GTW-CCS-EGR. For GTW-CCS, PCC-MEA absorbers require 5798 t/h of lean MEA, deliver decarbonated flue gas at 0.59% molCO_2 (1 atm/55 °C), and strip water-saturated CO_2 at 92.6% mol (1 atm/40 °C), consuming 776.4 MW of LPS, while the respective GTW-CCS-EGR values are 5319 t/h, 1.37% molCO_2 (1 atm/63 °C), 92.6% mol (1 atm/40 °C), and 749.3 MW. The PCC-MEA difference between GTW-CCS and GTW-CCS-EGR is the flue gas volume to absorbers. EGR reduces the flue gas flowrate by 55%, reducing the number of absorbers from 14 to 7 for the same 91.9% CO_2 capture. EGR PCC-MEA has higher flue gas CO_2 content (15.8% mol vs. 7.21% mol), entailing a higher absorption driving force and reducing the stage number (40 to 36), despite a 4% lower solvent capture ratio.

Table 7. PCC-MEA results of GTW-CCS and intensified GTW-CCS-EGR.

		GTW-CCS		GTW-CCS-EGR	
		Absorbers	**Strippers**	**Absorbers**	**Strippers**
Total Gas (Absorbers) or Liquid (Strippers) Inlet Flow rate	$MMm^{3,Std}/d$	99.3	1.6	45.1	2.00
	t/h	5099.1	6048.0	2389.1	5816.36
	kmol/h	174,934.5	245,909.2	79,530.5	236,621.88
$Stages^{Theoretical}$		40	20	36	20
Columns		14	7	7	7
Gas or Liquid Flow rate per Column (t/h)		348.8	864.0	359.4	830.9
Gas or Liquid Flow rate per Column (kmol/h)		12,495.3	35,129.9	11,361.5	33,803.1
Gas or Liquid Inlet % molCO_2		7.21%	6.22%	15.80%	6.36%
Gas^{Outlet} % molCO_2		0.59%	92.62%	1.37%	92.63%
Gas^{Outlet} T (°C)		56	40	63	40
$Liquid^{Outlet}$ T (°C)		52.02	110.82	61.44	110.78
Capture Ratio ($kg^{Solvent}/kg^{CO2}$)		10.4		10.0	
Heat Ratio (kJ/mol^{CO2})		241.3		233.2	
Reboiler Duty (MW)		776.4		749.3	
Total Gas^{Outlet} from Strippers (kmol/h)		12,506.3		12,486.9	
Total CO_2^{Outlet} from Strippers (t/h)		509.7		508.9	
CO_2 Capture Efficiency (% mol/mol)		91.93%		91.91%	
Packing (Stage Equivalent Height)		MELLAPAK 250X (0.6096m/stage)			
Packing Height (m) + Spacing (m) [60]		24.4 + 3	12.2 + 3	22 + 3	12.2 + 3
Columns Height (m)/Diameter (m)		27.4/6.1	15.2/3.3	25/5.9	15.2/3.4

This represents an impressive cost reduction—seven 36-staged absorbers versus fourteen 40-staged absorbers—that boosts GTW-CCS-EGR's economic evaluation. In GTW-CCS and GTW-CCS-EGR, dense CO_2 (300 bar/40 °C) is exported to EOR at 927 kg/m^3 after CO2-CMP#2 unit. GTW-CCS dispatches 509.7 t/h of CO_2-to-EOR, reaching a carbon-intensity of 0.080 t^{CO2}/MWh, while GTW-CCS-EGR dispatches 508.9 t/h of CO_2-to-EOR with 0.084 t^{CO2}/MWh.

The TEG dehydration unit removes ≈89% of water from water-saturated CO_2, producing 512.5 t/h (GTW-CCS) and 508.8 t/h (GTW-CCS-EGR) of dry CO_2 with ≈150 ppm H_2O. The TEG reboiler demands ≈0.59 MW of LPS duty and the injection of 0.61% of dry CO_2 (≈3 t/h) for keeping $T^{Reboiler}$ = 140 °C. Lean TEG is recovered at 98.5% *w*/*w*. Table 8 shows TEG dehydration results for GTW-CCS and GTW-CCS-EGR.

Offshore operations comprise NG compression to 200 bar and temperature swing adsorption for raw NG dehydration to 1 ppm-mol H_2O, aiming for zero gas hydrates in the NG pipeline. Temperature swing adsorption operates in cycles of 12 h adsorption and 4 h desorption, removing 0.40 t/h of H_2O and generating 6.5 $MMm^{3,Std}/d$ of treated NG (Table 1). The power consumption of NG compressors is added to the power demand of GTW-CONV, GTW-CCS, and GTW-CCS-EGR. The offshore rig provides costless utilities (heating and CW) for offshore operations.

Figure 10 displays pressure and velocity profiles through the submarine NG (rig-to-shore) and CO_2 (shore-to-field) pipelines for process GTW-CCS-EGR. These profiles agree with similar literature results [61]. The NG pipeline results are exactly the same for GTW-CONV, GTW-CCS, and GTW-CCS-EGR, since these processes have exactly the same NG demand. On the other hand, the CO_2 pipeline results only refer to the alternatives that implement CCS (GTW-CCS and GTW-CCS-EGR). In this case, the CO_2 pipeline results for GTW-CCS-EGR are approximately the same for GTW-CCS, since there are small differences in the CO_2-to-EOR flow rate and the purity for these processes (Table 8).

Table 8. TEG dehydration unit results.

TEG Results		GTW-CCS		GTW-CCS-EGR	
		Absorber	**Stripper**	**Absorber**	**Stripper**
Total Gas (Absorbers) or Liquid (Strippers) Inlet Flow rate	Actual_m^3/d	4921.0	3.9	4885.8	3.8
	t/h	513.4	2.9	509.7	2.9
	kmol/h	11,689.0	52.4	11,605.0	51.2
TEG^{Inlet} (%w/w)		98.5	73.1	98.5	72.7
TEG^{Outlet} (%w/w)		73.1	98.5	72.7	98.5
$Stages^{Theoretical}$		20	10	20	10
Columns		1	1	1	1
Wet CO_2 (ppm-mol H_2O)		1370.0	-	1369.4	-
Dry CO_2 (ppm-mol H_2O)		148.2	-	154.0	-
Gas^{Outlet} T (°C)		41.8	40.0	41.7	40.0
$Liquid^{Outlet}$ T (°C)		40.4	140.0	40.3	140.0
Dry CO_2 (kmol/h)		11,649.4		11,566.5	
Dry CO_2 to Reboiler (kmol/h)		71.44		70.4	
Reboiler Duty (MW)		0.593		0.590	
Packing (Stage Equivalent Height)		MELLAPAK 250X (0.6096 m/stage)			
Packing Height (m)		12.2	18.7	12.2	18.7
Extra Height (m) [60]		3.0	3.0	3.0	3.0
Column Height (m)		15.2	21.7	15.2	21.7
Diameter (m)		5.7	5.4	5.7	5.4

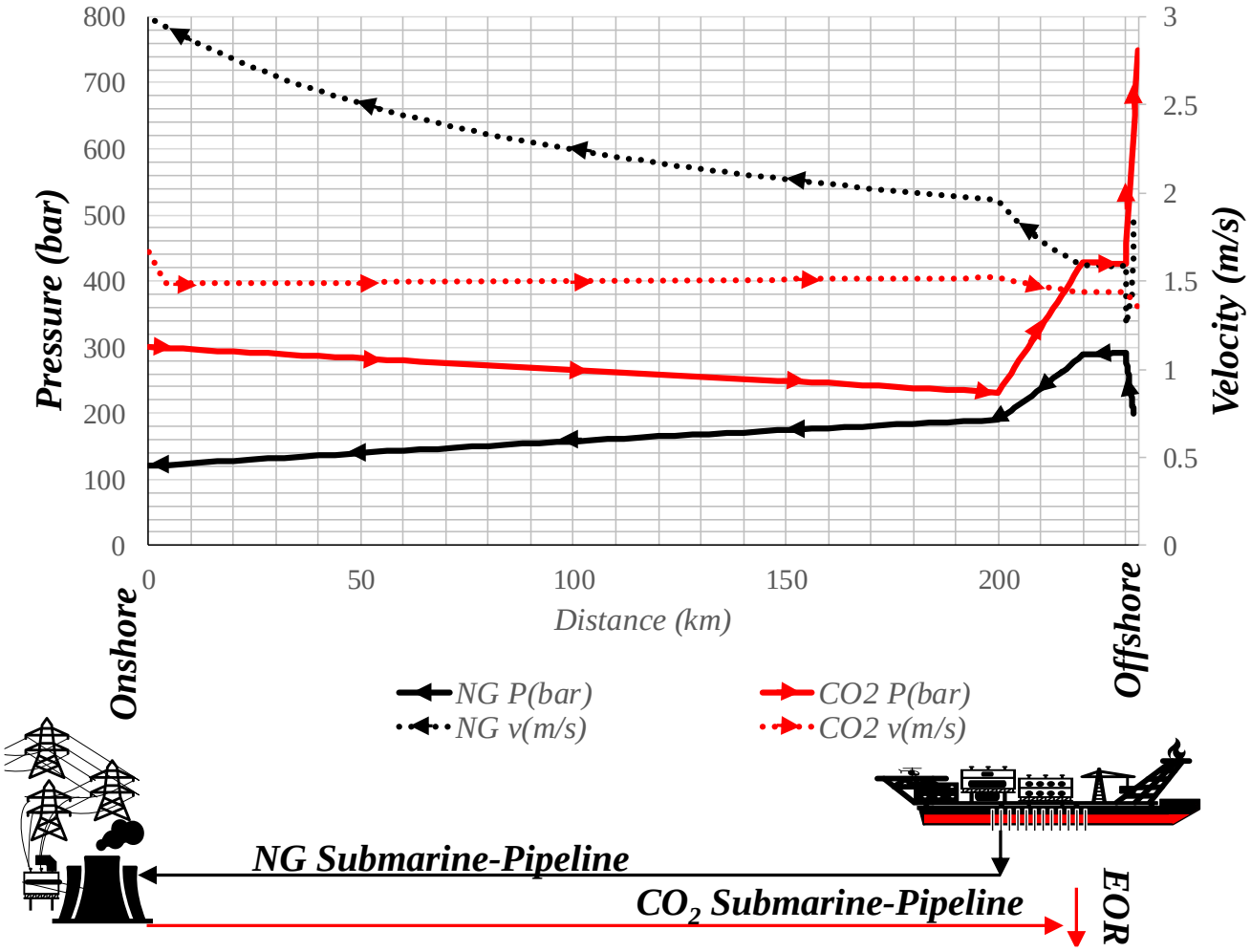

Figure 10. Pressure and velocity profiles of the NG and CO_2 pipelines of GTW-CCS-EGR.

Through the continental shelf segment (200 km), pressure drops from 300 bar to 230 bar (velocity = 1.55 m/s) in the CO_2 pipeline and from 190 bar to 120 bar ($velocity^{Max}$ = 3 m/s) in the NG pipeline. Through the continental slope segment (20 km, inclination = −10%), pressure increases from 230 bar to 430 bar in the CO_2 pipeline and drops from 288 bar to 190 bar in the NG pipeline. Through the submarine plateau segment (10 km), pressure drops from 430 bar to 425 bar in the CO_2 pipeline and from 290 bar to 288 bar in the NG pipeline. Through the NG downcomers (2 km, inclination = −100%), pressure increases from 200 bar to 290 bar. Lastly, pressure increases from 425 bar to 745 bar through the CO_2 injection column (3 km, inclination = −100%).

3.2. Multi-Criteria Sustainability Analysis Results

Figure 11 depicts the 17 indicator (Table 4) results of the multi-criteria sustainability analysis of GTW-CONV, GTW-CCS, and GTW-CCS-EGR. The global energy dimension scores are 86%, 75%, and 75%, respectively, for GTW-CONV, GTW-CCS, and GTW-CCS-EGR. GTW-CONV has a better energy performance due to the CCS penalty of GTW-CCS and GTW-CCS-EGR. On the other hand, GTW-CCS and GTW-CCS-EGR attained much better carbon intensity scores due to CCS, despite worse *HS* and *HSv* scores associated with MEA, TEG, and liquid CO_2. The global environment dimension scores are 40%, 72%, and 72%, respectively, for GTW-CONV, GTW-CCS, and GTW-CCS-EGR, while the respective global economic dimension scores (oil price USD 80/bbl) attain 49%, 50%, and 50% and the respective global material efficiency scores attain 89%, 83%, and 85%. It is worth remarking that all cases have similar economic percentage scores *CRMy*, *TR*, *payback period* (*DPBP*), *NPV*, and *COM*.

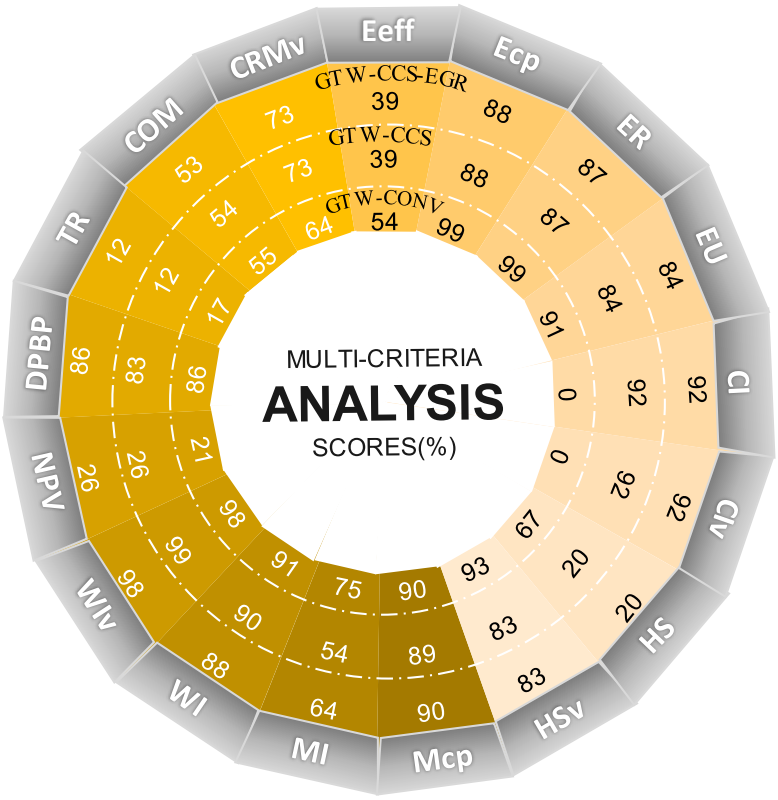

Figure 11. Multi-criteria analysis of GTW-CONV, GTW-CCS, and GTW-CCS-EGR.

3.3. Thermodynamic Analysis Results

Thermodynamic analysis comprises the overall GTW-CCS and GTW-CCS-EGR systems and the following eight sub-systems: (i) NGCC; (ii) DCC; (iii) PCC-MEA; (iv) CO_2-CMP#1; (v) CO_2-CMP#2; (vi) TEG; (vii) STR-CO2; and (viii) CW tower. The CO2-CMP

was divided into the following two sub-systems: before (CO_2-CMP#1) and after (CO_2-CMP#2) TEG dehydration. Maximum power, equivalent power, and thermodynamic efficiency were calculated for overall systems and sixteen sub-systems, resulting in eighteen thermodynamic analyses. Figure 12 depicts the sub-systems analyzed for GTW-CCS and GTW-CCS-EGR with respective feed streams, product streams, and utilities consumptions (C_{LPS} and EE, respectively, mean LPS condensate and electricity produced/consumed). The EGR indication in Figure 12 is valid only for the GTW-CCS-EGR. Offshore operations—TSA unit, NG-compressors, and pipelines—were not considered in the thermodynamic analysis.

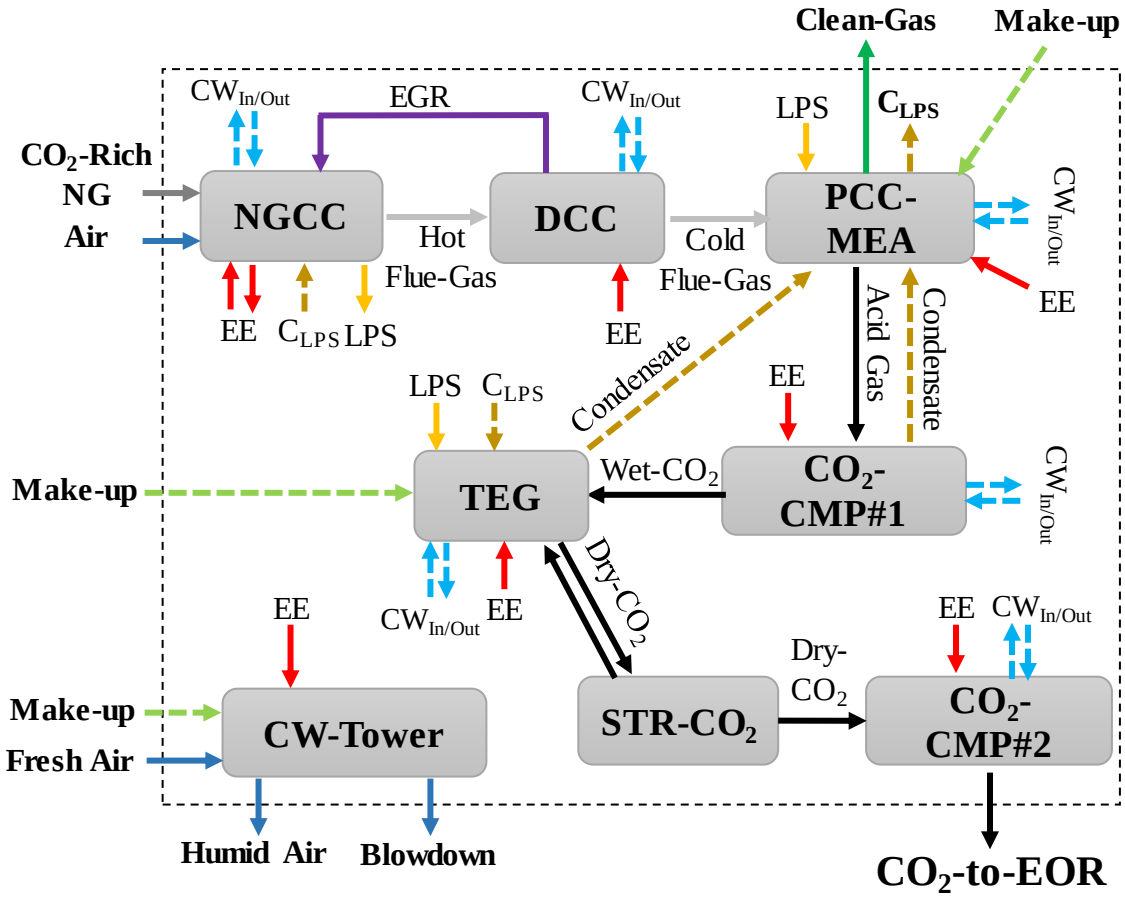

Figure 12. Thermodynamic analysis of boundaries of GTW-CCS, GTW-CCS-EGR, and their sub-systems.

Before presenting the results of the thermodynamic analysis and to exemplify the first and second laws of thermodynamics in the present context, Table 9 shows stream properties for a reasonably complex open system belonging to GTW-CCS-EGR, namely the HRSG. As can be seen, the HRSG exhibits a positive entropy creation rate with a magnitude around 9% of the entropy traffic, confirming the second law for a steady-state adiabatic system. The HRSG operation also confirms the principle of energy conservation for the open system (i.e., the first law), showing a very small residue of 0.0000032%, compatible with the magnitude of numerical errors expected in professional process simulators.

Table 10 presents the results of the second law analysis for overall systems GTW-CCS, GTW-CCS-EGR, and their sub-systems (note that the thermodynamic analysis of GTW-CONV corresponds to the thermodynamic analysis of the NGCC sub-system of GTW-CCS). Only PCC-MEA, CO_2-CMP#1 and #2, and the TEG sub-system are power-consuming systems ($\dot{W}^{MAX} < 0$). Thus, the thermodynamic analysis for these sub-systems uses Equations (19a), (20a), (21a), (22a), and (23b). All remaining sub-systems (and the overall systems) are power-producing systems ($\dot{W}^{MAX} > 0$) and should adopt Equations (19b), (20b), (21b), (22b), and (23c) in the thermodynamic analysis. Equation (14) is applied in

all $\dot{W}^{MAX}$ calculations. PCC-MEA, TEG, and CO_2-CMP are power-consuming systems because compression and CO_2 or H_2O removal are not spontaneous processes and must be driven by power and heat consumptions. The comparison of overall GTW-CCS and GTW-CCS-EGR thermodynamic efficiencies and their respective sub-systems are presented in Figure 13.

Table 9. Thermodynamic and transport properties of HRSG streams—validation of the first and second laws of thermodynamics for HRSG in GTW-CCS-EGR.

Unit	Streams of HRSG	Type	Flow Rate (kmol/h)	Enthalpy (kJ/kmol)	Entropy (kJ/kmol.K)	Viscosity (cP)	Thermal Conductivity (W/m.K)
HRSG	Hot Flue gas	Input	180,738.1	−65,989.0	197.2	0.0390	0.0629
	CO_2-Rich NG	Input	11,459.9	−216,542.8	162.8	0.0138	0.0272
	LPS Condensate	Input	71,061.5	−276,785.2	30.1	0.2051	0.6879
	HPS Condensate	Input	2800.0	−283,666.9	10.5	0.6393	0.6327
	MPS1 to reheat	Input	3200.0	−229,848.0	125.8	0.0231	0.0526
	MPS1 Condensate	Input	400.0	−283,834.0	10.3	0.6486	0.6318
	MPS2 Condensate	Input	400.0	−283,878.6	10.3	0.6514	0.6315
	Cold Flue gas	Output	180,738.1	−82,746.9	175.9	0.0222	0.0322
	Hot CO_2-Rich NG	Output	11,459.9	−213,940.3	170.6	0.0161	0.0337
	LPS	Output	71,061.5	−237,809.1	126.0	0.0133	0.0272
	HPS	Output	2800.0	−224,314.7	122.0	0.0308	0.0806
	MPS1 reheated	Output	3200.0	−223,048.8	135.3	0.0300	0.0737
	MPS1	Output	400.0	−234,428.4	117.9	0.0181	0.0420
	MPS2	Output	400.0	−229,956.7	139.6	0.0225	0.0487
First and Second Laws Verification for HRSG		**Unit**					
(1) Total Entropy Input Rate		kJ/K.h	40,089,973.7				
(2) Total Entropy Output Rate		kJ/K.h	43,570,121.7				
Entropy Creation Rate: (2) — (1)		kJ/K.h	+3,480,147.9 (+8.8%)				
(3) Total Enthalpy Input Rate		kJ/h	−35,833,920,242.3				
(4) Total Enthalpy Output Rate		kJ/h	−35,833,921,391.9				
(5) Total Heat Absorbed		kJ/h	0.0				
(6) Total Power Exported		kJ/h	0.0				
First Law Residue: (3) + (5) — (4) — (6)		kJ/h	+1149.6 (+0.0000032%)				

The NGCC sub-system is a power-producing system, since it performs spontaneous transformations. This is confirmed by its positive $\dot{W}^{MAX}$ = 1672.4 MW. Its $|\dot{W}^{Eq}|$= 845.4 MW derives from (i) $\dot{W}^{Eq}_{CW}$ = 1.3 MW associated with the Rankine cycle condenser; (ii) $\dot{W}^{Eq}_{LPS}$ = 207.3 MW from LPS produced in the HRSG as utility; and (iii) $E\dot{E}$ = 636.8 MW resulting from gas turbines and Rankine cycle net power. The EGR intensification in the NGCC imposes a reduction in all these values—$\dot{W}^{MAX}$ = 1642.9 MW , $|\dot{W}^{Eq}|$ = 835.1 MW, $E\dot{E}$ = 628.1 MW , and $\dot{W}^{Eq}_{LPS}$ = 204.4 MW—except in the $\dot{W}^{Eq}_{CW}$, which increases to 2.61 MW. The thermodynamic efficiency of the NGCC sub-system is 50.6% ($\eta > 0$) and slightly increases to 50.8% after EGR implementation. It should be noted that superheated steam does not entail equivalent power terms because the HPS and MPS (different from LPS) are not exported through NGCC boundaries.

The DCC presents similar performances both with and without EGR. LPS is not consumed, $\dot{W}^{Eq}_{LPS} = 0$, and CW is a process stream that is not considered a utility ($\dot{W}^{Eq}_{CW} = 0$). That is, cold CW is considered as a feed stream and hot CW is considered as a product stream for $\dot{W}^{MAX}$ calculation with Equation (14). For this reason, $|\dot{W}^{Eq}|$ is exclusively related to electricity consumption in CW pumps. Despite the positive $\dot{W}^{MAX}$ values for both DCCs,

their thermodynamic efficiencies are negative, since there is no power generation (instead, electricity is consumed in the pumps), indicating a wasted thermodynamic potential.

Table 10. Second law analysis of GTW-CCS, GTW-CCS-EGR, and their sub-systems.

System	$\dot{W}^{MAX}$ (MW)	$\dot{W}^{Eq}_{CW}$ (MW)	$\dot{W}^{Eq}_{LPS}$ (MW)	$E\dot{E}$ (MW)	$\lvert \dot{W}^{Eq} \rvert$ (MW)	η%	$\dot{W}^{LOST\ \&}$ (MW)	$\dot{W}^{LOST\ \#}$ (MW)	$\dot{W}^{LOST}$ Divergence (%)
GTW-CCS									
NGCC	1672.31	1.27	207.27	636.82	845.36	50.6	826.95	826.96	0.001
DCC	38.00	–	–	−1.40	−1.40	−3.7	39.40	39.37	0.08
PCC-MEA	−61.31	−35.26	206.93	0.61	172.28	35.6	110.97	110.26	0.64
CO_2-CMP#1	−28.63	−4.19	–	49.46	45.27	63.2	16.64	16.60	0.23
CO_2-CMP#1	−5.40	−2.76	–	14.51	11.76	46.0	6.35	6.33	0.38
TEG	−0.00008	−0.03	0.16	0.0036	0.13	0.06	0.13	0.13	0.58
STR-CO_2	0.1701	–	–	–	0	0	0.17	0.17	0.03
CWT	24.48	–	–	−8.81	−8.81	−36.0	33.29	33.27	0.06
Sum Crosscheck	1639.62	–	–	–	–	–	1033.91	1033.09	0.08
Overall System	**1600.64**	**–**	**–**	**562.50**	**562.50**	**35.14**	**1038.14**	**1030.89**	**0.70**
GTW-CCS-EGR									
NGCC-EGR	1642.90	2.61	204.41	628.07	835.09	50.8	807.81	805.67	0.26
DCC	32.52	–	–	−1.40	−1.40	−4.3	33.92	33.96	0.10
PCC-MEA	−52.09	−35.88	200.51	0.56	165.19	31.5	113.10	112.92	0.16
CO2-CMP#1	−28.40	−4.16	–	49.08	44.92	63.2	16.51	16.48	0.20
CO_2-CMP#2	−5.36	−2.74	–	14.40	11.66	46.0	6.30	6.30	0.03
TEG	−0.0001	−0.03	0.16	0.004	0.13	0.04	0.13	0.13	0.59
STR-CO2	0.1699	–	–	–	0	0	0.17	0.17	0.00
CWT	25.06	–	–	−9.03	−9.03	−36.0	34.09	33.89	0.60
Sum Crosscheck	1614.62	–	–	–	–	–	1012.04	1009.52	0.25
Overall System	**1566.44**	–	**–**	**553.56**	**553.56**	**35.34**	**1012.88**	**1013.90**	0.10

[&] via Equations (22a) and (22b); [#] via Equations (23b) and (23c).

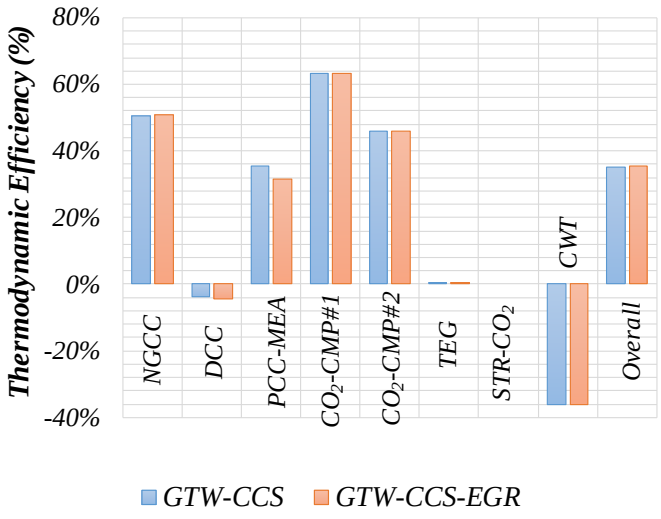

Figure 13. Thermodynamic efficiencies of overall GTW-CSS, GTW-CCS-EGR, and their sub-systems.

PCC-MEA presented a negative $\dot{W}^{MAX}$, and $|\dot{W}^{Eq}| = 172.2$ MW for GTW-CCS associated with $\dot{W}^{Eq}_{CW} = -35.3$ MW, due to the stripper condenser and lean solvent cooler. For GTW-CCS-EGR, the respective values are $|\dot{W}^{Eq}| = 165.2$ MW and $\dot{W}^{Eq}_{CW} = -35.88$ MW. The $\dot{W}^{Eq}_{LPS} = 206.9$ MW from LPS consumption in the stripper reboiler, and the $E\dot{E} = 0.6$ MW from the solvent recirculation pump and water make-up pump are slightly higher for

GTW-CCS compared to GTW-CCS-EGR ($\dot{W}_{LPS}^{Eq}$ = 200.5 MW, $E\dot{E}$ = 0.56 MW). As a power-consuming system, the PCC-MEA thermodynamic efficiency is calculated through Equation (21a), resulting in *35.6%* for GTW-CCS and *31.5%* for GTW-CCS-EGR.

Similar to PCC-MEA, CO_2-CMP#1 (upstream CO_2 dehydration) and CO_2-CMP#2 (downstream CO_2 dehydration) are also power-consuming systems and present negative $\dot{W}^{MAX}$ because they perform non-spontaneous compression. For GTW-CCS, $|\dot{W}^{Eq}|$ reaches 45.27 MW and 11.76 MW for CO_2-CMP#1 and CO_2-CMP#2, respectively; while for GTW-CCS-EGR, the corresponding $|\dot{W}^{Eq}|$ values are 44.9 MW and 11.6 MW for CO_2-CMP#1 and CO_2-CMP#2, respectively. LPS utility is not consumed in this sub-system ($\dot{W}_{LPS}^{Eq} = 0$). For GTW-CCS, the $\dot{W}_{CW}^{Eq}$ of -4.19 MW and -2.76 MW correspond to the intercoolers of CO_2-CMP#1 and CO_2-CMP#2, respectively, while the $E\dot{E}$ values of 49.46 MW and 14.51 MW represent electricity consumption by compressors and pumps in CO_2-CMP#1 and CO_2-CMP#2, respectively. GTW-CCS-EGR presents corresponding similar results, with a $\dot{W}_{CW}^{Eq}$ of -4.16 MW and -2.74 MW, and an $E\dot{E}$ of 49.08 MW and 14.40 MW for CO_2-CMP#1 and CO_2-CMP#2, respectively. The thermodynamic efficiency via Equation (21a) results in the same values of 63.2% (CO_2-CMP#1) and 46.0% (CO-CMP#2) for both GTW-CCS and GTW-CCS-EGR.

The CW tower is a power-producing system with positive $\dot{W}^{MAX}$ and negative $|\dot{W}^{Eq}|$ due to the electricity consumption ($E\dot{E}$) associated with pumps and blower. Consequently, this system has a negative thermodynamic efficiency ($\eta < 0$). LPS is not consumed ($\dot{W}_{LPS}^{Eq} = 0$) and CW is not considered a utility ($\dot{W}_{CW}^{Eq} = 0$). The negative efficiencies of -36.0% in both cases of CW tower system unveil a huge unfulfilled thermodynamic potential.

The TEG unit is also a power-consumer system with negative $\dot{W}^{MAX}$ and $|\dot{W}^{Eq}|$ of 0.13 MW, which is associated with $\dot{W}_{LPS}^{Eq} = 0.16$ MW from LPS for the stripper reboiler and an $E\dot{E}$ of 0.004 MW from the TEG recirculation pump and make-up pump. The thermodynamic efficiency corresponds to 0.06% and 0.04% for GTW-CCS and GTW-CCS-EGR.

STR-CO2 is a power-producing system with a positive $\dot{W}^{MAX}$ of 0.17 MW. LPS, CW, and $E\dot{E}$ are not consumed ($\dot{W}_{LPS}^{Eq} = 0$, $\dot{W}_{CW}^{Eq} = 0$, $E\dot{E} = 0$), resulting in a 0% thermodynamic efficiency in both GTW-CCS and GTW-CCS-EGR.

Finally, the thermodynamic analyses consider the respective overall systems GTW-CCS and GTW-CCS-EGR. The analysis of the overall systems does not include CW and LPS loops since they lie entirely within system boundaries. GTW-CCS and GTW-CCS-EGR are power-producing systems with hugely positive $\dot{W}^{MAX}$ values. Then, the thermodynamic efficiencies are calculated with $\dot{W}^{Eq} > 0$, using Equation (19b), resulting in thermodynamic efficiencies of 35.14% for GTW-CCS and 35.34% for GTW-CCS-EGR.

Lost work determination offers insights about where, how, and how much power potential is destroyed in the overall system and in each sub-system. The results presented in Table 10 compares the lost work results obtained from the following two different and independent methods: (i) using $\dot{W}^{MAX}$ and $|\dot{W}^{Eq}|$ from Equations (22a) and (22b) and (ii) via the $T_0\dot{S}^{UNIV}$ product in Equation (21a), which turns into Equation (23b) for power-consuming systems and Equation (23c) for power-producing systems. As a consistency crosscheck, the sum of the lost work results of all sub-systems should recover the overall GTW-CCS or GTW-CCS-EGR lost work. In fact, slightly discrepant values are typically observed in this sum crosscheck, as well as in the $T_0\dot{S}^{UNIV}$ check.

As demonstrated in Table 10, $\dot{W}^{LOST}$ values calculated via Equations (22a) and (22b) are consistent; that is, these results were validated through the second law crosscheck in Equations (23b) and (23c), since all discrepancies were found to be lower than *1%*. These

slight divergences are expected and can be attributed to round-off errors, convergence tolerances in process recycling, and the complex numerical nature of the simulation of huge processes in professional simulators. Additionally, the process simulation involves multiple transitions across thermodynamic packages, contributing to these minor divergences in $\dot{W}^{LOST}$ crosschecks.

Sankey diagrams are built in Figure 14 to illustrate $\dot{W}^{LOST}$ flows through overall GTW-CCS, overall GTW-CCS-EGR, and their individual sub-systems. The sum of individual lost work values from their sub-systems determines the overall $\dot{W}^{LOST}$ (as indicated in the sum crosscheck of Table 10), while $\Delta\dot{W}^{LOST}$ represents the difference between the lost work values calculated for the overall system through the two different ways indicated in Table 10.

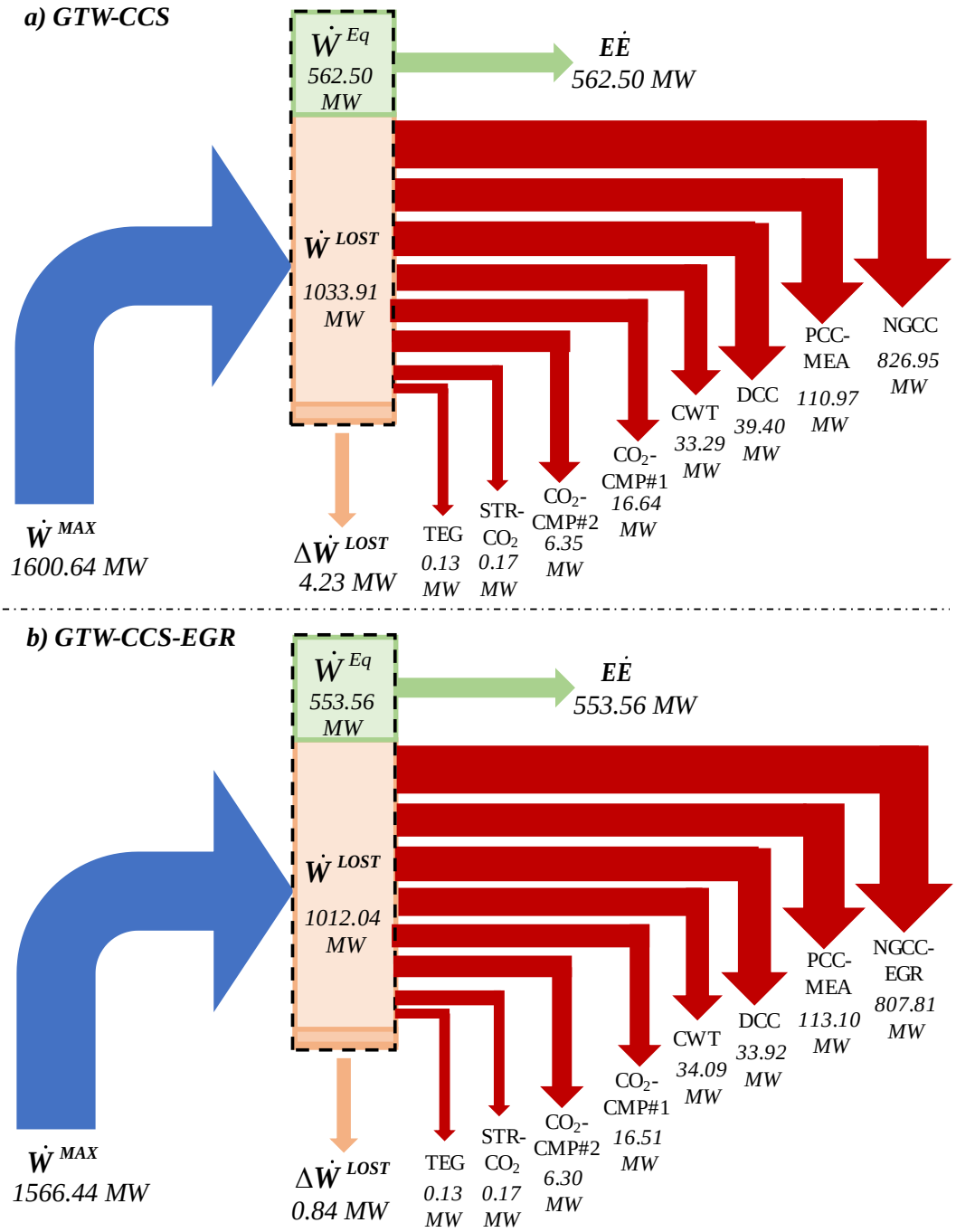

Figure 14. Lost work Sankey diagrams. (**a**) GTW-CCS and (**b**) GTW-CCS-EGR.

From 1600.64 MW of power availability ($\dot{W}^{MAX}$) of the GTW-CCS, 64.6% is lost in the process. The NGCC sub-system attained the greatest $\dot{W}^{LOST}$ share (826.95 MW or 79.98%), seconded by the PCC-MEA sub-system (110.97 MW or 10.73%), followed by DCC (39.40 MW or 3.81%), CWT (33.29 MW or 3.22%), CO_2-CMP#1 (16.64 MW or 1.61%), CO_2-CMP#2 (6.35 MW or 0.61%), STR-CO_2 (0.17 MW or 0.016%), and TEG (0.13 MW or 0.012%). For the GTW-CCS-EGR, the NGCC sub-system attained the greatest $\dot{W}^{LOST}$ share (807.81 MW or 79.81%), seconded by the PCC-MEA sub-system (113.10 MW or 11.18%), followed by DCC (33.92 MW or 3.35%), CWT (34.09 MW or 3.36%), CO_2-CMP#1 (16.51 MW or 1.63%), CO_2-CMP#2 (6.30 MW or 0.62%), STR-CO_2 (0.17 MW or 0.016%), and TEG (0.13 MW or 0.012%).

3.4. Economic Analysis

For 80 USD/bbl oil price, GTW-CONV, GTW-CCS, and GTW-CCS-EGR economic performances were assessed in terms of *COM*, *FCI*, *REV*, and *NPV*, considering the 30 years horizon in Table 11. GTW-CONV economic results reached $FCI^{GTW\text{-}CONV}$ = 990.02 MMUSD, $NPV^{GTW\text{-}CONV}$ = 1416.53 MMUSD (payback time = 6 years), evincing the lowest investment due to the absence of PCC-MEA, CO_2 pipeline, and compressors. For the two CCS cases, the investment reached $FCI^{GTW\text{-}CCS}$ = 1611.44 MMUSD and $FCI^{GTW\text{-}CCS\text{-}EGR}$ = 1558.50 MMUSD, showing that EGR and Rankine Cycle intensifications greatly lowered PCC-MEA *FCI*—despite a small increase in NGCC *FCI*—somewhat increasing the final *NPV*. Figure 15 depicts *NPV* versus time for GTW-CONV, GTW-CCS, and GTW-CCS-EGR.

Table 11. Investment (*FCI*), net present value (*NPV*), and other economic variables.

Onshore *FCI* Items (MMUSD)		**GTW-CONV**	**GTW-CCS**	**GTW-CCS-EGR**
NGCC		153.05	135.15	139.84
DCC		16.40	16.40	16.40
PCC-MEA		-	113.99	49.74
CO2-CMP		-	27.53	27.52
TEG + STR-CO2		-	6.64	6.64
CW Tower		8.24	9.39	9.58
Onshore Total *FCI* (MMUSD)		177.69	309.10	249.71
Offshore *FCI* Items (MMUSD)	Pipelines	720.00	1210.00	1210.00
	NG Downcomer	16.00	16.00	16.00
	NG Dehydration	18.66	18.66	18.66
	NG Compression	57.68	57.68	57.68
Offshore Total *FCI* (MMUSD)		990.02	1611.44	1552.04
DEPR (MMUSD/y)		99.00	161.14	155.20
COM (MMUSD/y)		364.02	475.88	465.20
Revenues (MMUSD/y)	Power Exported	731.49	469.18	461.47
	CO_2-to-EOR	-	514.58	509.85
GAP (MMUSD/y)		367.47	507.87	506.12
AP (MMUSD/y)		276.19	346.73	386.81
NPV (MMUSD)		1416.53	1798.28	1827.40
Payback Time (y)		5.90	6.90	6.68

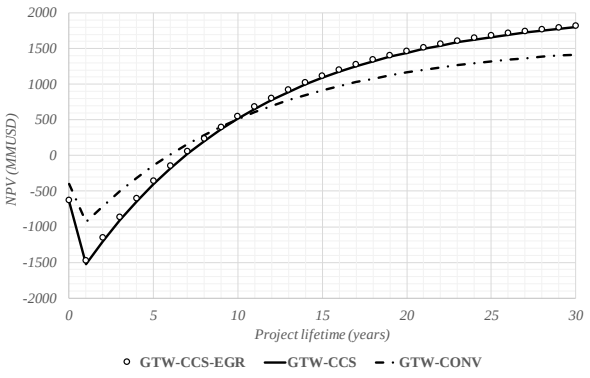

Figure 15. *NPV* vs. time for GTW-CONV, GTW-CCS, and GTW-CCS-EGR.

4. Conclusions

A low carbon emission and intensified GTW-CCS-EGR process—executing post-combustion capture via aqueous MEA absorption with exhaust gas recycle and firing CO_2-rich NG from remote oil/gas fields—was assessed on technical, economic, and thermodynamic grounds. The process-intensified case, GTW-CCS-EGR, was compared with two other more conventional cases, (i) GTW-CCS, which lacks the exhaust gas recycle; and (ii) GTW-CONV without implementing carbon capture and storage and intensifications (the benchmark conventional case). Evidently, the GTW-CONV is better in the power exported aspect. However, GTW-CCS-EGR is thermodynamically, economically, and environmentally the best for processing CO_2-rich NG.

GTW-CONV fed with 6.5 $MMSm^3/d$ of CO_2-rich NG produces 863.38 MW as surplus electricity, while GTW-CCS-EGR produces 553.56 MW (64.10% of GTW-CONV net power). On the other hand, GTW-CCS-EGR captures 505.8 t/h of CO_2, which results in an emission factor of 0.084 tCO_2/MWh, while the same value for GTW-CONV reaches 0.642 tCO_2/MWh.

The PCC-MEA plant removes ≈92% of the CO_2 in the flue gas. The captured CO_2 is compressed and sent to EOR. This high-pressure CO_2 is practically pure and dehydrated (99.95% mol $CO_2 \approx 150$ ppmH_2O) and it is assumed to be traded at 1.5 $bblOil/tCO_2$, generating extra revenue. In this scenario, the GTW-CCS-EGR is economically feasible with positive $NPV^{30years}$ of 1829 MMUSD in a realistic scenario of 80 USD/bbl of oil price.

In the economic and environmental dimensions, the GTW-CCS-EGR presents better performance for *NPV* and carbon intensity. However, the inclusion of MEA, TEG, and liquid CO_2 in the component list of GTW-CCS-EGR results in a slightly greater environmental score for GTW-CONV. In terms of material and energy dimensions, GTW-CONV shows better global scores, evidencing the impact of CCS cost and CCS penalty on gas-to-wire processes.

The second law analysis of GTW-CCS-EGR showed that its overall thermodynamic efficiency reached 35.34%, against 35.14% for the GTW-CCS and 50.6% for the NGCC subsystem. The sub-systems PCC-MEA, TEG, and CO_2-CMP are the only power-consuming systems in GTW-CCS-EGR, demanding different formulas for thermodynamic efficiency and equivalent power in the analysis. The consistency of the GTW-CCS-EGR thermodynamic analysis was confirmed through two crosschecks embedded in lost work calculation, namely (i) sum crosscheck, i.e., the sum of $\dot{W}^{LOST}$ values of the individual sub-systems matches the overall system $\dot{W}^{LOST}$ and (ii) $\dot{W}^{LOST}$ of each sub-system and overall system match independent $\dot{W}^{LOST}$ estimates through the well-known formula $T_0\dot{S}^{UNIV}$ from the second law of thermodynamics. Lost work analysis also pinpointed the greatest sinks of equivalent power destruction, namely the NGCC sub-system (79.81%), followed by PCC-MEA (11.18%).

In summary, the main contribution of this work was to disclose and evaluate a strategy for the process intensification of low-emission gas-to-wire processes burning CO_2-rich NG available at remote oil/gas fields and using the captured CO_2 as an EOR agent in the same field. This is the proposed GTW-CCS-EGR intensified low-emission gas-to-wire process. Moreover, GTW-CCS-EGR was fully assessed on thermodynamic, technical, and economic grounds, establishing not only its feasibility but also its globally superior performance compared to GTW-CONV and GTW-CCS.

5. Suggestions for Future Work

Suggestions for future work aim at eliminating some lacunae in this study, such as (i) to include offshore operations—pipelines, TSA, and NG-compressors—in the thermodynamic analysis; (ii) to implement the evaluation of public policies such as the carbon market, charging CO_2 taxes, and potential increases in fossil fuel prices; (iii) to incorporate these critical topics in the economic evaluation; and (iv) to consider the impact of energy security, accounting for the new electricity supply to the grid. In this last regard, it is worth mentioning that the GTW-CCS-EGR process is a reliable and secure supply of electricity

that enhances the resilience and sustainability of the energy infrastructure since it does not depend on climatic seasonality and operates at stationary conditions.

Author Contributions: I.B.S.P.: Software, Writing—Original Draft, Validation, Investigation, Data Curation, Visualization, Writing—Review and Editing, Formal Analysis. O.d.Q.F.A.: Supervision, Project Administration, Writing—Review and Editing. J.L.d.M.: Conceptualization, Software, Methodology, Investigation, Supervision, Writing—Original Draft, Writing—Review and Editing, Visualization, Formal Analysis. All authors have read and agreed to the published version of the manuscript.

Funding: J.L. de Medeiros and O.Q.F. Araújo acknowledge support from CNPq Brazil (313861/2020-0, 312328/2021-4) and from FAPERJ Brazil (E-26/200.522/2023, E-26/201.178/2021). I.B.S. Poblete acknowledges support from FAPERJ Brazil. (E-26/205.985/2022, E-26/205.984/2022).

Data Availability Statement: Data are contained within the article.

Conflicts of Interest: The authors declare no conflicts of interest.

Abbreviations

CCS: carbon capture and storage; CE: Carnot engine; CHP: Carnot heat pump; CW: cooling water; DCC: direct contact column; EGR: exhaust gas recycle; EOR: enhanced oil recovery; HPS: high-pressure steam; HRSG: heat recovery steam generator; LPS: low-pressure saturated steam; LHV: lower heating value; MPS: medium-pressure steam; MMUSD: million US Dollar; NG: natural sas; NGCC: NG combined cycle; PCC-MEA: post-combustion capture with aqueous monoethanolamine; PR-EOS: Peng–Robinson equation of state; TEG: triethylene-glycol.

Nomenclature

AP, *GAP*	Net and gross annual profits (MMUSD/y)
COL, *COM*	Costs of labor and of manufacturing (MMUSD/y)
CBM	Bare module costs (MMUSD)
CF	Capacity factor (MW, m^2, or m^3)
$\overline{C}_P^{\,CW}$	Isobaric heat capacity of water (J/mol.K)
CEPCI	Chemical Engineering Plant Cost Index
CRM	Cost of raw materials (MMUSD/y)
CUT, *DEPR*	Cost of utilities and depreciation (MMUSD/y)
DPBP	Discounted Payback Time (y)
$E\dot{E}$	Electricity (MW)
Fn	*n*th Feed stream flow rate (kmol/s)
FCI	Fixed Capital Investment (MMUSD)
$\overline{H}$	Molar enthalpy (MJ/kmol)
HR	Heat Ratio (kJ/kg^{CO2})
ITR, *i*	Income tax rate, annual interest rate (%)
NEQ	Number of equipment items
NF, *NK*	Numbers of feed streams and product streams
NPV	Net present value (MMUSD)
Kn	*n*th product stream flow rate (kmol/s)
$\dot{Q}$	Heat duty (MW)
REV	Revenues (MMUSD/y)
$\overline{S}$	Molar entropy (MJ/kmol.K)
T	Absolute temperature (K)
$\dot{W}$	Power (MW)
η	Thermodynamic efficiency (%)

References

1. Kotagodahetti, R.; Hewage, K.; Perera, P.; Sadiq, R. Technology and Policy Options for Decarbonizing the Natural Gas Industry: A Critical Review. *Gas Sci. Eng.* **2023**, *114*, 204981. [CrossRef]
2. United Nations Framework Convention on Climate Change (UNFCCC). Kyoto Protocol to the UNFCCC. Available online: https://unfccc.int/resource/docs/convkp/kpeng.pdf (accessed on 13 February 2024).
3. Ellerman, A.D.; Buchner, B.K. The European Union Emissions Trading Scheme: Origins, Allocation, and Early Results. *Rev. Environ. Econ. Policy* **2007**, *1*, 66–87. [CrossRef]
4. United Nations Framework Convention on Climate Change (UNFCCC). Paris Agreement. Available online: https://unfccc.int/sites/default/files/english_paris_agreement.pdf (accessed on 13 February 2024).

5. Budinis, S.; Krevor, S.; Dowell, N.M.; Brandon, N.; Hawkes, A. An Assessment of CCS Costs, Barriers and Potential. *Energy Strateg. Rev.* **2018**, *22*, 61–81. [CrossRef]
6. Guo, J.-X.; Huang, C.; Wang, J.-L.; Meng, X.-Y. Integrated Operation for the Planning of CO2 Capture Path in CCS–EOR Project. *J. Pet. Sci. Eng.* **2020**, *186*, 106720. [CrossRef]
7. Rao, A.D. Natural Gas-Fired Combined Cycle (NGCC) Systems. In *Combined Cycle Systems for Near-Zero Emission Power Generation*; Elsevier: Amsterdam, The Netherlands, 2012; pp. 103–128, ISBN 978-0-85709-013-3.
8. Hekmatmehr, H.; Esmaeili, A.; Pourmahdi, M.; Atashrouz, S.; Abedi, A.; Ali Abuswer, M.; Nedeljkovic, D.; Latifi, M.; Farag, S.; Mohaddespour, A. Carbon Capture Technologies: A Review on Technology Readiness Level. *Fuel* **2024**, *363*, 130898. [CrossRef]
9. Carapellucci, R.; Giordano, L.; Vaccarelli, M. Study of a Natural Gas Combined Cycle with Multi-Stage Membrane Systems for CO2 Post-Combustion Capture. *Energy Procedia* **2015**, *81*, 412–421. [CrossRef]
10. Khan, B.A.; Ullah, A.; Saleem, M.W.; Khan, A.N.; Faiq, M.; Haris, M. Energy Minimization in Piperazine Promoted MDEA-Based CO_2 Capture Process. *Sustainability* **2020**, *12*, 8524. [CrossRef]
11. Ab Rahim, A.H.; Yunus, N.M.; Bustam, M.A. Ionic Liquids Hybridization for Carbon Dioxide Capture: A Review. *Molecules* **2023**, *28*, 7091. [CrossRef] [PubMed]
12. Grasa, G.S.; Abanades, J.C. CO_2 Capture Capacity of CaO in Long Series of Carbonation/Calcination Cycles. *Ind. Eng. Chem. Res.* **2006**, *45*, 8846–8851. [CrossRef]
13. Theo, W.L.; Lim, J.S.; Hashim, H.; Mustaffa, A.A.; Ho, W.S. Review of Pre-Combustion Capture and Ionic Liquid in Carbon Capture and Storage. *Appl. Energy* **2016**, *183*, 1633–1663. [CrossRef]
14. Darabkhani, H.G.; Varasteh, H.; Bazooyar, B. Oxyturbine Power Cycles and Gas-CCS Technologies. In *Carbon Capture Technologies for Gas-Turbine-Based Power Plants*; Darabkhani, H.G., Varasteh, H., Eds.; Elsevier: Amsterdam, The Netherlands, 2023; pp. 39–74, ISBN 978-0-12-818868-2.
15. Davoodi, S.; Al-Shargabi, M.; Wood, D.A.; Rukavishnikov, V.S.; Minaev, K.M. Review of Technological Progress in Carbon Dioxide Capture, Storage, and Utilization. *Gas Sci. Eng.* **2023**, *117*, 205070. [CrossRef]
16. Wang, M.; Lawal, A.; Stephenson, P.; Sidders, J.; Ramshaw, C. Post-Combustion CO_2 Capture with Chemical Absorption: A State-of-the-Art Review. *Chem. Eng. Res. Des.* **2011**, *89*, 1609–1624. [CrossRef]
17. Plaza, J.M.; Van Wagener, D.; Rochelle, G.T. Modeling CO_2 Capture with Aqueous Monoethanolamine. *Int. J. Greenh. Gas Control* **2010**, *4*, 161–166. [CrossRef]
18. Valenti, G.; Bonalumi, D.; Macchi, E. Energy and Exergy Analyses for the Carbon Capture with the Chilled Ammonia Process (CAP). *Energy Procedia* **2009**, *1*, 1059–1066. [CrossRef]
19. Peeters, A.N.M.; Faaij, A.P.C.; Turkenburg, W.C. Techno-Economic Analysis of Natural Gas Combined Cycles with Post-Combustion CO2 Absorption, Including a Detailed Evaluation of the Development Potential. *Int. J. Greenh. Gas Control* **2007**, *1*, 396–417. [CrossRef]
20. Tait, P.; Buschle, B.; Ausner, I.; Valluri, P.; Wehrli, M.; Lucquiaud, M. A Pilot-Scale Study of Dynamic Response Scenarios for the Flexible Operation of Post-Combustion CO_2 Capture. *Int. J. Greenh. Gas Control* **2016**, *48*, 216–233. [CrossRef]
21. Schach, M.-O.; Schneider, R.; Schramm, H.; Repke, J.-U. Techno-Economic Analysis of Postcombustion Processes for the Capture of Carbon Dioxide from Power Plant Flue Gas. *Ind. Eng. Chem. Res.* **2010**, *49*, 2363–2370. [CrossRef]
22. Luo, X.; Wang, M. Optimal Operation of MEA-Based Post-Combustion Carbon Capture for Natural Gas Combined Cycle Power Plants under Different Market Conditions. *Int. J. Greenh. Gas Control* **2016**, *48*, 312–320. [CrossRef]
23. Bao, J.; Zhang, L.; Song, C.; Zhang, N.; Guo, M.; Zhang, X. Reduction of Efficiency Penalty for a Natural Gas Combined Cycle Power Plant with Post-Combustion CO_2 Capture: Integration of Liquid Natural Gas Cold Energy. *Energy Convers. Manag.* **2019**, *198*, 111852. [CrossRef]
24. Cormos, C.-C. Assessment of Chemical Absorption/Adsorption for Post-Combustion CO_2 Capture from Natural Gas Combined Cycle (NGCC) Power Plants. *Appl. Therm. Eng.* **2015**, *82*, 120–128. [CrossRef]
25. Garcia, S.; Fernandez, E.S.; Stewart, A.J.; Maroto-Valer, M.M. Process Integration of Post-Combustion CO_2 Capture with Li_4SiO_4/Li_2CO_3 Looping in a NGCC Plant. *Energy Procedia* **2017**, *114*, 2611–2617. [CrossRef]
26. Zhang, W.; Sun, C.; Snape, C.E.; Sun, X.; Liu, H. Cyclic Performance Evaluation of a Polyethylenimine/Silica Adsorbent with Steam Regeneration Using Simulated NGCC Flue Gas and Actual Flue Gas of a Gas-Fired Boiler in a Bubbling Fluidized Bed Reactor. *Int. J. Greenh. Gas Control* **2020**, *95*, 102975. [CrossRef]
27. Roussanaly, S.; Aasen, A.; Anantharaman, R.; Danielsen, B.; Jakobsen, J.; Heme-De-Lacotte, L.; Neji, G.; Sødal, A.; Wahl, P.E.; Vrana, T.K.; et al. Offshore Power Generation with Carbon Capture and Storage to Decarbonise Mainland Electricity and Offshore Oil and Gas Installations: A Techno-Economic Analysis. *Appl. Energy* **2019**, *233–234*, 478–494. [CrossRef]
28. Brito, T.L.F.; Galvão, C.; Fonseca, A.F.; Costa, H.K.M.; Moutinho dos Santos, E. A Review of Gas-to-Wire (GtW) Projects Worldwide: State-of-Art and Developments. *Energy Policy* **2022**, *163*, 112859. [CrossRef]
29. Flórez-Orrego, D.; Albuquerque, C.; da Silva, J.A.M.; Freire, R.L.A.; de Oliveira Junior, S. Optimal Design of Power Hubs for Offshore Petroleum Platforms. *Energy* **2021**, *235*, 121353. [CrossRef]
30. Orisaremi, K.K.; Chan, F.T.S.; Chung, N.S.H. Potential Reductions in Global Gas Flaring for Determining the Optimal Sizing of Gas-to-Wire (GTW) Process: An Inverse DEA Approach. *J. Nat. Gas Sci. Eng.* **2021**, *93*, 103995. [CrossRef]
31. Jokar, S.M.; Wood, D.A.; Sinehbaghizadeh, S.; Parvasi, P.; Javanmardi, J. Transformation of Associated Natural Gas into Valuable Products to Avoid Gas Wastage in the Form of Flaring. *J. Nat. Gas Sci. Eng.* **2021**, *94*, 104078. [CrossRef]

32. Henningsen, S. Air Pollution from Large Two-Stroke Diesel Engines and Technologies to Control It. In *Handbook of Air Pollution from Internal Combustion Engines*; Sher, E.B.T.-H., Ed.; Elsevier: San Diego, CA, USA, 1998; pp. 477–534, ISBN 978-0-12-639855-7.
33. Okubo, M.; Kuwahara, T. Principle and Design of Emission Control Systems. In *New Technologies for Emission Control in Marine Diesel Engines*; Okubo, M., Kuwahara, T.B.T.-N.T., Eds.; Elsevier: Amsterdam, The Netherlands, 2020; pp. 53–143, ISBN 978-0-12-812307-2.
34. Alcaráz-Calderon, A.M.; González-Díaz, M.O.; Mendez, Á.; González-Santaló, J.M.; González-Díaz, A. Natural Gas Combined Cycle with Exhaust Gas Recirculation and CO_2 Capture at Part-Load Operation. *J. Energy Inst.* **2019**, *92*, 370–381. [CrossRef]
35. Hachem, J.; Schuhler, T.; Orhon, D.; Cuif-Sjostrand, M.; Zoughaib, A.; Molière, M. Exhaust Gas Recirculation Applied to Single-Shaft Gas Turbines: An Energy and Exergy Approach. *Energy* **2022**, *238*, 121656. [CrossRef]
36. Ali, U.; Agbonghae, E.O.; Hughes, K.J.; Ingham, D.B.; Ma, L.; Pourkashanian, M. Techno-Economic Process Design of a Commercial-Scale Amine-Based CO_2 Capture System for Natural Gas Combined Cycle Power Plant with Exhaust Gas Recirculation. *Appl. Therm. Eng.* **2016**, *103*, 747–758. [CrossRef]
37. Lee, W.-S.; Kang, J.-H.; Lee, J.-C.; Lee, C.-H. Enhancement of Energy Efficiency by Exhaust Gas Recirculation with Oxygen-Rich Combustion in a Natural Gas Combined Cycle with a Carbon Capture Process. *Energy* **2020**, *200*, 117586. [CrossRef]
38. Nanadegani, F.S.; Sunden, B. Review of Exergy and Energy Analysis of Fuel Cells. *Int. J. Hydrogen Energy* **2023**, *48*, 32875–32942. [CrossRef]
39. Nie, X.; Xue, J.; Zhao, L.; Deng, S.; Xiong, H. New Insight of Thermodynamic Cycle in Thermoelectric Power Generation Analyses: Literature Review and Perspectives. *Energy* **2024**, *292*, 130553. [CrossRef]
40. Geuzebroek, F.H.; Schneiders, L.H.J.M.; Kraaijveld, G.J.C.; Feron, P.H.M. Exergy Analysis of Alkanolamine-Based CO2 Removal Unit with AspenPlus. *Energy* **2004**, *29*, 1241–1248. [CrossRef]
41. Gülen, S.C.; Smith, R.W. Second Law Efficiency of the Rankine Bottoming Cycle of a Combined Cycle Power Plant. *J. Eng. Gas Turbines Power* **2010**, *132*, 011801. [CrossRef]
42. Brigagão, G.V.; Arinelli, L.D.O.; de Medeiros, J.L.; Araújo, O.d.Q.F. Low-Pressure Supersonic Separator with Finishing Adsorption: Higher Exergy Efficiency in Air Pre-Purification for Cryogenic Fractionation. *Sep. Purif. Technol.* **2020**, *248*, 116969. [CrossRef]
43. Cruz, M.D.A.; de Araújo, O.Q.F.; de Medeiros, J.L. Exergy Comparison of Single-Shaft and Multiple-Paralleled Compressor Schemes in Offshore Processing of CO2-Rich Natural Gas. *J. Nat. Gas Sci. Eng.* **2020**, *81*, 103390. [CrossRef]
44. Wiesberg, I.L.; Brigagão, G.V.; Araújo, O.D.Q.F.; de Medeiros, J.L. Carbon Dioxide Management via Exergy-Based Sustainability Assessment: Carbon Capture and Storage versus Conversion to Methanol. *Renew. Sustain. Energy Rev.* **2019**, *112*, 720–732. [CrossRef]
45. Milão, R.D.F.D.; Carminati, H.B.; de Araújo, O.Q.F.; de Medeiros, J.L. Thermodynamic, Financial and Resource Assessments of a Large-Scale Sugarcane-Biorefinery: Prelude of Full Bioenergy Carbon Capture and Storage Scenario. *Renew. Sustain. Energy Rev.* **2019**, *113*, 109251. [CrossRef]
46. Talebizadehsardari, P.; Ehyaei, M.A.; Ahmadi, A.; Jamali, D.H.; Shirmohammadi, R.; Eyvazian, A.; Ghasemi, A.; Rosen, M.A. Energy, Exergy, Economic, Exergoeconomic, and Exergoenvironmental (5E) Analyses of a Triple Cycle with Carbon Capture. *J. CO2 Util.* **2020**, *41*, 101258. [CrossRef]
47. Amrollahi, Z.; Ertesvåg, I.S.; Bolland, O. Optimized Process Configurations of Post-Combustion CO_2 Capture for Natural-Gas-Fired Power Plant—Exergy Analysis. *Int. J. Greenh. Gas Control* **2011**, *5*, 1393–1405. [CrossRef]
48. Minutillo, M.; Lubrano Lavadera, A.; Jannelli, E. Assessment of Design and Operating Parameters for a Small Compressed Air Energy Storage System Integrated with a Stand-Alone Renewable Power Plant. *J. Energy Storag.* **2015**, *4*, 135–144. [CrossRef]
49. Souza, I.V.A.F.; Ellis, G.S.; Ferreira, A.A.; Guzzo, J.V.P.; Díaz, R.A.; Albuquerque, A.L.S.; Amrani, A. Geochemical Characterization of Natural Gases in the Pre-Salt Section of the Santos Basin (Brazil) Focused on Hydrocarbons and Volatile Organic Sulfur Compounds. *Mar. Pet. Geol.* **2022**, *144*, 105763. [CrossRef]
50. General Electric (GE). GE Gas&Power—Gas Turbines 9F. Available online: https://www.ge.com/gas-power/products/gas-turbines/9f (accessed on 13 February 2024).
51. Turton, R. *Analysis, Synthesis, and Design of Chemical Processes*; Prentice-Hall International Series in Engineering; Prentice Hall: Hoboken, NJ, USA, 2012; ISBN 9780132618120.
52. Chemical Engineering (CE). The Chemical Engineering Plant Cost Index. Available online: https://www.chemengonline.com/Assets/File/CEPCI_2002.pdf (accessed on 13 February 2024).
53. Carminati, H.B.; Milão, R.D.F.D.; de Medeiros, J.L.; de Araújo, O.Q.F. Bioenergy and Full Carbon Dioxide Sinking in Sugarcane-Biorefinery with Post-Combustion Capture and Storage: Techno-Economic Feasibility. *Appl. Energy* **2019**, *254*, 113633. [CrossRef]
54. U.S. Energy Information Administration (EIA). Natural Gas Henry Hub Spot Price: Average of 2022. Available online: https://www.eia.gov/dnav/ng/hist/rngwhhdm.htm (accessed on 13 February 2024).
55. U.S. Energy Information Administration (EIA). Independent Statistics and Analysis. Electricity and Natural Gas Data Browser: Average of 2022. Available online: https://www.eia.gov/electricity/data/browser/#/topic/7?agg=2,0,1&geo=g&freq=M (accessed on 13 February 2024).
56. Thorne, R.J.; Sundseth, K.; Bouman, E.; Czarnowska, L.; Mathisen, A.; Skagestad, R.; Stanek, W.; Pacyna, J.M.; Pacyna, E.G. Technical and Environmental Viability of a European CO2 EOR System. *Int. J. Greenh. Gas Control* **2020**, *92*, 102857. [CrossRef]
57. Liptak, B. Optimization of Cooling Towers. Available online: https://www.controlglobal.com/manage/optimization/article/11304737/optimization-of-cooling-towers (accessed on 13 February 2024).
58. Ruiz-Mercado, G.J.; Smith, R.L.; Gonzalez, M.A. Sustainability Indicators for Chemical Processes: I. Taxonomy. *Ind. Eng. Chem. Res.* **2012**, *51*, 2309–2328. [CrossRef]

59. Aspentech. 2024. Aspen Technology Inc. Available online: www.aspentech.com/en/about-aspentech (accessed on 1 March 2024).
60. Mcampbell, J. Gas Conditioning and Processing. *J. Chem. Inf. Model.* **2013**, *53*, 1689–1699.
61. Kim, S. Maximum Allowable Fluid Velocity and Concern on Piping Stability of ITER Tokamak Cooling Water System. *Fusion Eng. Des.* **2021**, *162*, 112049. [CrossRef]

Disclaimer/Publisher's Note: The statements, opinions and data contained in all publications are solely those of the individual author(s) and contributor(s) and not of MDPI and/or the editor(s). MDPI and/or the editor(s) disclaim responsibility for any injury to people or property resulting from any ideas, methods, instructions or products referred to in the content.